BRAIN
A JOURNAL OF NEUROLOGY

Protection of primary neurons and mouse brain from Alzheimer's pathology by molecular tweezers

Aida Attar,[1,2] Cristian Ripoli,[3] Elisa Riccardi,[3] Panchanan Maiti,[1] Domenica D. Li Puma,[3] Tingyu Liu,[1] Jane Hayes,[1] Mychica R. Jones,[1,4] Kristin Lichti-Kaiser,[5] Fusheng Yang,[1,4] Greg D. Gale,[6] Chi-hong Tseng,[7] Miao Tan,[8] Cui-Wei Xie,[2,8] Jeffrey L. Straudinger,[5] Frank-Gerrit Klärner,[9] Thomas Schrader,[9] Sally A. Frautschy,[1,4] Claudio Grassi[3] and Gal Bitan[1,2,10]

1 Department of Neurology, University of California at Los Angeles, Los Angeles, CA 90095, USA
2 Brain Research Institute, University of California at Los Angeles, Los Angeles, CA 90095, USA
3 Institute of Human Physiology, Università Cattolica, Rome 00168, Italy
4 Greater Los Angeles Healthcare System, Veterans Hospital, North Hills, CA 91343, USA
5 Department of Pharmacology and Toxicology, University of Kansas, Lawrence, KS 66045, USA
6 Department of Molecular and Medical Pharmacology, University of California at Los Angeles, Los Angeles, CA 90095, USA
7 Department of Medicine, David Geffen School of Medicine, University of California at Los Angeles, Los Angeles, CA 90095, USA
8 Department of Psychiatry and Biobehavioural Sciences, University of California at Los Angeles, Los Angeles, CA 90095, USA
9 Institute of Organic Chemistry, University of Duisburg-Essen, Essen 45117, Germany
10 Molecular Biology Institute, University of California at Los Angeles, Los Angeles, CA 90095, USA

Correspondence to: Gal Bitan,
Department of Neurology,
David Geffen School of Medicine,
University of California at Los Angeles,
Neuroscience Research Building 1, Room 451,
635 Charles E. Young Drive South,
Los Angeles, CA 90095-7334, USA
E-mail: gbitan@mednet.ucla.edu

Alzheimer's disease is a devastating cureless neurodegenerative disorder affecting >35 million people worldwide. The disease is caused by toxic oligomers and aggregates of amyloid β protein and the microtubule-associated protein tau. Recently, the Lys-specific molecular tweezer CLR01 has been shown to inhibit aggregation and toxicity of multiple amyloidogenic proteins, including amyloid β protein and tau, by disrupting key interactions involved in the assembly process. Following up on these encouraging findings, here, we asked whether CLR01 could protect primary neurons from Alzheimer's disease-associated synaptotoxicity and reduce Alzheimer's disease–like pathology in vivo. Using cell culture and brain slices, we found that CLR01 effectively inhibited synaptotoxicity induced by the 42-residue isoform of amyloid β protein, including ~80% inhibition of changes in dendritic spines density and long-term potentiation and complete inhibition of changes in basal synaptic activity. Using a radiolabelled version of the compound, we found that CLR01 crossed the mouse blood–brain barrier at ~2% of blood levels. Treatment of 15-month-old triple-transgenic mice for 1 month with CLR01 resulted in a decrease in brain amyloid β protein aggregates, hyperphosphorylated tau and microglia load as observed by immunohistochemistry. Importantly, no signs of toxicity were observed in the treated mice, and CLR01 treatment did not affect the amyloidogenic processing of amyloid β protein precursor. Examining induction or inhibition of the cytochrome P450 metabolism system by CLR01 revealed minimal interaction. Together, these data suggest that CLR01 is safe for use at concentrations well above those showing efficacy in mice. The efficacy and toxicity results support a process-specific mechanism of action of molecular tweezers and suggest that these are promising compounds for developing disease-modifying therapy for Alzheimer's disease and related disorders.

Introduction

Alzheimer's disease is the leading cause of dementia, affecting >35 million people worldwide (Alzheimer's Association, 2011). Neuropathologically, Alzheimer's disease is characterized by accumulation of neuritic plaques, comprising mainly fibrillar amyloid β protein and neurofibrillary tangles made of filamentous hyperphosphorylated tau (p-tau). The inceptive assault on susceptible neurons is believed to be mediated by amyloid β and possibly tau oligomers that disrupt synaptic communication (Kirkitadze *et al.*, 2002; Kayed, 2010) before cognitive symptoms can be detected. Thus, if formation of these toxic assemblies can be prevented before overt neurodegeneration occurs, the brain may be able to mount a defence and possibly recover.

We sought compounds that would modulate the assembly of amyloid β and tau and inhibit their toxicity at the earliest possible step. We identified Lys residues as attractive targets where interference would disrupt assembly because these residues have a unique ability to participate in both hydrophobic and electrostatic interactions involved in the assembly process of amyloidogenic proteins, including amyloid β and tau (Petkova *et al.*, 2002; Lazo *et al.*, 2005; Huang and Stultz, 2008; Li *et al.*, 2009; Usui *et al.*, 2009; Cohen *et al.*, 2011; Vana *et al.*, 2011; Sinha *et al.*, 2012b). Therefore, we conjectured that compounds that bind specifically to Lys residues might inhibit formation of toxic amyloid β and tau assemblies.

Lys-specific 'molecular tweezers', originally reported by Fokkens *et al.* (2005), bind to Lys residues with a dissociation constant of ~20 µM. Their specificity for Lys results from the Lys butylene moiety threading through the molecular tweezer cavity and facilitating hydrophobic interactions with the molecular tweezer sidewalls, and the ε-ammonium group's electrostatic attraction to the negatively charged bridgehead groups of the molecular tweezers. Thus, molecular tweezers use the same types of interactions involved in early amyloid β assembly (Lazo *et al.*, 2005), allowing them to compete with these interactions and disrupt amyloid β assembly and toxicity. A similar mechanism is expected to inhibit tau toxicity.

Recently, we have shown that a molecular tweezer derivative called CLR01 is a potent inhibitor of assembly and toxicity of multiple disease–related amyloidogenic proteins, including amyloid β and tau (Sinha *et al.*, 2011). CLR01 was found to inhibit amyloid β oligomerization, dissociate preformed amyloid β fibrils and stabilize non-toxic amorphous assemblies. Mass spectrometry and nuclear magnetic resonance experiments confirmed binding of CLR01 to Lys in amyloid β at the earliest stages of assembly (Sinha *et al.*, 2011). CLR01 was found to inhibit amyloid β–induced toxicity in differentiated rat pheochromocytoma cells and in primary rat hippocampal cultures or mixed neuronal/glial cultures (Sinha *et al.*, 2012a) at micromolar concentrations. In addition, CLR01 was found to rescue zebrafish expressing human wild-type α-synuclein from severe deformation and early

death by keeping the intracellular α-synuclein soluble and allowing its proteasomal clearance (Prabhudesai *et al.*, 2012).

In light of these encouraging results, we evaluated the effect of CLR01 on synaptic dysfunction *in vitro* and on Alzheimer's disease–related brain pathology in transgenic mice. We also studied several aspects of CLR01's drug-like characteristics and possible toxicity to evaluate the potential of molecular tweezers as mechanism-based drugs for Alzheimer's disease and related diseases. The initial assessment described here suggests that CLR01 is an efficacious and safe drug lead.

Materials and methods

Additional details on methods are available in the online Supplementary material.

Molecular tweezers

CLR01 and CLR03 were prepared and purified as described previously (Talbiersky *et al.*, 2008).

Protein and sample preparation

The 42-residue isoform of amyloid β (amyloid β_{42}) was obtained from the University of California–Los Angeles Biopolymers Laboratory or from AnaSpec. Sample preparation was performed as described previously (Maiti *et al.*, 2010). Briefly, amyloid β_{42} was disaggregated by treatment with 1,1,1,3,3,3-hexafluoroisopropanol (Sigma) as described (Rahimi *et al.*, 2009). Dried peptide films were stored at −20°C until use. For dendritic spine experiments, 27-µg films were dissolved in 20 µl of 60 mM sodium hydroxide, sonicated for 1 min, and then diluted to 30 µM with 180 µl of Neurobasal® media. For electrophysiological experiments, 50-µg films were dissolved in 11 µl of dimethyl sulphoxide to reach a concentration of 1 mM and sonicated for 10 min. For basal synaptic transmission experiments, 2 µl of the solution was then diluted to 5 ml with culture media to reach a final concentration of 400 nM. For long-term potentiation experiments, 40 µl of amyloid β_{42} from 100 µM stock solution was incubated for 12 h at 4°C to promote protein oligomerization. This preparation was further diluted with artificial CSF in the absence or presence of CLR01 to reach the final amyloid β_{42} concentration of 200 nM immediately before experiments.

Primary hippocampal neuronal culture

Hippocampal neurons were prepared as described previously (Maiti *et al.*, 2010) and plated on poly-D-Lys-coated (0.1 mg/ml) 13-mm round glass cover slips in 24-well culture plates at a density of 300 000 cells/well.

Dendritic spine morphology

Experiments were performed as described previously (Maiti *et al.*, 2010). Briefly, rat primary hippocampal neurons were grown for

3 weeks. Half of the growth medium (1 ml) was removed and new media (600 μl) containing 30 μM freshly prepared amyloid β_{42} (200 μl) and media containing 300 μM CLR01 or CLR03 (200 μl) were immediately added, resulting in a final concentration of 3 μM amyloid β_{42} and 30 μM CLR01 or CLR03. After 72 h of incubation, neurons were fixed with 4% paraformaldehyde and stained with 1,1'-dioctadecyl-3,3,3',3'-tetramethylindocarbocyanine perchlorate (DiI, Invitrogen). The neurons were visualized using a confocal laser-scanning microscope (Leica) at ×2000 magnification. The total number of spines per 100 μm were counted using ImageJ (Abramoff *et al.*, 2004). At least 100 dendritic branches from 10 to 15 individual neurons were selected per experimental condition. All data are shown as means ± standard error measure, and the level of significance was set at $P < 0.05$. Statistical analysis was performed in Prism 5.0c (GraphPad) using one-way ANOVA with Tukey's *post hoc* multiple-comparison test.

Autaptic neuron culture preparation and synaptic transmission studies

Basal synaptic transmission was studied in autaptic microcultures of hippocampal neurons using the patch-clamp technique in the whole-cell configuration, as described previously (Ripoli *et al.*, 2012). Briefly, neurons were voltage clamped at a membrane potential (V_m) of −70 mV, and stimuli mimicking action potentials (2 ms at 0 mV) were delivered every 6 s to evoke excitatory postsynaptic currents. The amplitudes and frequency of miniature excitatory postsynaptic currents were evaluated in 60-s recordings ($V_m = -70$ mV). The detection threshold of miniature excitatory postsynaptic currents was set to 3.5 times the baseline standard deviation. These parameters were measured in cells exposed for 24 h to freshly prepared 200 nM amyloid β_{42}, 200 nM amyloid β_{42} + 2 μM CLR01, or vehicle. Amyloid β_{42} (2 μl from 1 mM stock solution in dimethyl sulphoxide) was mixed with 20 μl of CLR01 (from 1 mM stock solution in water) and diluted up to 5 ml to the final concentrations of 400 nM and 4 μM of amyloid β_{42} and CLR01, respectively. Medium (5 ml) was removed and replaced with 5 ml of fresh media containing dimethyl sulphoxide vehicle, amyloid β_{42} alone or amyloid β_{42} and CLR01. Additional details are provided in the Supplementary material.

Long-term potentiation recordings

Electrophysiological recordings were performed using standard protocols in coronal hippocampal slices (400-μm thick) obtained from 8-week-old male C57BL/6 mice as described previously (Fusco *et al.*, 2012). Briefly, field excitatory postsynaptic potential (field EPSP) evoked by Schaffer collateral stimulation was recorded from the CA1 subfield of the hippocampus. The stimulation intensity that produced one-third of the maximal response was used for the test pulses, and the long-term potentiation-induction protocol consisted of four trains of 50 stimuli at 100 Hz repeated every 20 s, hereto called the 'high-frequency stimulation' paradigm. The magnitude of long-term potentiation was measured for 60 min after tetanus and expressed as a percentage of baseline field EPSP peak amplitude. The mean values observed during the last 10 min of pre-tetanus recordings were considered to represent the baseline at 100%. For experiments, 40 μl of amyloid β_{42} from 100 μM stock solution and 40 μl of CLR01 from 1 mM stock solution were mixed and either immediately diluted to a final volume of 20 ml, corresponding to final amyloid β_{42} concentration 200 nM and final CLR01 concentration 2 μM, or incubated for 1 h and then diluted. The diluted mixture was then immediately added to slices

and incubated for 20 min followed by long-term potentiation induction with a standard high-frequency stimulation paradigm. Additional details are provided in the Supplementary material. Statistical analysis in all electrophysiological experiments (Student's unpaired *t*-test) was performed with SYSTAT 10.2 (Statcom).

Western blot analysis of amyloid β_{42} species under electrophysiological experimental conditions

The assembly size of the amyloid β_{42} species was analysed in both denaturing and native conditions using Western blots probed with anti-amyloid β monoclonal antibody 6E10. Amyloid-β_{42} preparations for these analyses were identical to those in the electrophysiological experiments described earlier. See Supplementary material for additional details.

Blood–brain barrier experiments

Three wild-type and three transgenic mice were anaesthetized by intraperitoneal injection of ketamine and xylazine. Then, 2 μCi/g of ^{3}H-CLR01 as a 11.8 μg/g of ^{3}H-CLR01 + CLR01 mixture, where the ^{3}H-CLR01 made up 10% of the total CLR01, was injected into the jugular vein. Mice remained anaesthetized for 1 h after injection, at which point blood was collected via cardiac puncture, the mouse perfused thoroughly through the heart with PBS and the brain collected. One hemisphere of the brain or 100–350 μl of blood were digested with 1 ml Solvable™ (Perkin Elmer), added to Ultima Gold™ liquid scintillation cocktail (Perkin Elmer) and read in a Triathler liquid scintillation counter (model 425-034). Brain penetration percentage was calculated as activity per gram of brain relative to activity per millilitre of blood. Statistical analysis (Student's unpaired *t*-test) was performed using Prism 5.0d (GraphPad).

Treatment of triple-transgenic mice with CLR01

Triple-transgenic mice (14–15 months old, $n = 6$–7) and wild-type control mice ($n = 11$–12) were anaesthetized with 3% isoflurane gas (oxygen 2 l/min) and mini-osmotic pumps (model 1004, Alzet) were subcutaneously implanted on the dorsal back. The pumps contained CLR01 in sterile saline (40 μg/kg/d) or saline as vehicle. The 40 μg/kg/d dose was chosen based on limited knowledge, at the time this experiment was initiated, of the solubility and safety of CLR01. On Day 28, mice were anaesthetized with pentobarbital (100 mg/kg), and blood was collected by cardiac puncture. Mice were perfused with cold non-fixative saline buffer containing protease and phosphatase inhibitors (Roche) as described previously (Lim *et al.*, 2000).

Immunohistochemistry

Analysis was performed according to previously published protocols (Lim *et al.*, 2000; Frautschy *et al.*, 2001). Paraffin-embedded mouse brain regions from −2.97 to −3.08 bregma were deparaffinized, and endogenous peroxidase activity was quenched with 0.3% hydrogen peroxide in methanol. The tissue was steamed for 60 min in 2% citrate-buffered antigen-unmasking solution (Vector Labs). Sections were blocked with Tris-buffered saline containing 5% normal horse serum (Vector Labs), 3% bovine serum albumin, and 0.1% Tween-20 and antibodies were diluted in the same solution. Sections

were incubated with monoclonal antibody 6E10 (Covance) diluted 1:1000, anti–p-tau monoclonal antibody AT8 (Thermo Scientific) for phosphorylated paired helical filaments diluted 1:45, anti-tau monoclonal antibody HT7 (Thermo Scientific) for total tau diluted 1:1000, anti-Iba1 polyclonal antibody for microglia (Wako) diluted 1:1000 or anti–glial fibrillary acidic protein monoclonal antibody for astrocytes (Sigma) diluted 1:5000 at 37°C for 1 h and then overnight at 4°C. This was followed by incubation with a secondary biotinylated anti-mouse immunoglobulin-G (Vector Labs) diluted 1:1200 for 6E10, AT8, HT7, and 1:3000 for glial fibrillary acidic protein, or biotinylated anti-rabbit immunoglobulin-G diluted 1:1000 for Iba1 in 1.5% normal horse serum with 3% bovine serum albumin in Tris-buffered saline with 0.1% Tween-20 for 1 h at 37°C. Slides were then incubated with an avidin:biotinylated enzyme complex (ABC Elite Vectastain® kit, Vector Labs) using a peroxidase detection system for 80 min at 37°C as described previously (Frautschy *et al.*, 2001). Antigen was visualized using metal-enhanced 3,3′-diaminobenzidine tetrahydrochloride (Thermo Scientific). Microscopic quantification used images analysed with macros written in-house for NIH-Image (http://rsb.info.nih.gov/nih-image) or ImageJ (http://rsbweb.nih.gov/ij/) to assess deposit size and number. Linear mixed effects models were used to evaluate the treatment effect on the outcome of amyloid β and p-tau load (see Supplementary material for details). For analysis of total tau, microglia and astrocytes, statistical analyses (Student's unpaired *t*-test) were performed using Prism 5.0d (GraphPad).

Mouse behavioural analysis

General activity and exploratory behaviour were assessed during a single 7-min session and quantified using an automated tracking system (EthoVision 3.0) as described previously (Gale *et al.*, 2009). Multiple locomotor-based endpoints, including velocity (cm/s), mobility (% time) and meander (°/cm), were quantified. Habituation rates for each endpoint were quantified by calculating the per cent change between the observed mean during the initial 90 s interval and the final 90 s interval. Statistical analysis for all endpoints was performed using two-way (treatment, genotype) ANOVA.

Brain extraction and western blot for amyloid β protein precursor cleavage products

Relevant brain regions (hippocampus, entorhinal and piriform cortices) were dissected out of one hemisphere of CLR01- or vehicle-treated triple-transgenic mouse brains at euthanasia. Brain regions were sonicated in a volume of Tris-buffered saline (20 mM Tris–HCl, 150 mM NaCl, pH 7.4) four to seven times the tissue weight, then pelleted at 157 000*g* for 15 min at 4°C. The supernatant was saved as the soluble fraction. The pellet was homogenized in Tris-buffered saline with 1% Triton™ X-100 and pelleted again. The supernatant was saved as the detergent-soluble fraction. Both fractions were subjected to a bicinchoninic acid protein assay (Thermo Fisher Scientific) following the manufacturer's protocol. The soluble fraction was fractionated on 10% Tris-Tricine SDS-PAGE gels and subjected to western blot using monoclonal antibody 22C11 (Millipore), which recognizes the N-terminal region of amyloid β protein precursor at 1:1000 dilution. The detergent-soluble fraction was fractionated on 10–20% gradient Tris-Tricine gels (Invitrogen) and subjected to western blot analysis probed with polyclonal antibody APP369 (Buxbaum *et al.*, 1990), specific for the C-terminal region of amyloid β protein precursor at 1:1000

dilution. All blots were stripped and re-probed with an anti-β-actin polyclonal antibody (AbFrontier) at 1:2000 dilution as a loading control. Blots were visualized using Enhanced Chemiluminescence (GE Healthcare) and bands quantified densitometrically using ImageJ. Statistical analysis (two-way ANOVA for treatment and genotype) was performed using Prism 5.0d (GraphPad).

CLR01 stability and cytochrome P450 inhibition

In vitro evaluation of CLR01's stability in plasma and liver microsomes, and inhibition of cytochrome P450 was performed by Wolfe Laboratories, Inc. The experimental details are proprietary and therefore only a brief description of each experiment is given. For stability measurements, CLR01 was incubated with mouse or human plasma or liver microsomes and an Nicotinamide adenine dinucleotide phosphate (NADPH)-regenerating system. Testing was conducted at 15 min intervals up to 60 min. After protein precipitation by an organic solvent, samples were analysed by high-performance liquid chromatography/mass spectrometry to determine overall stability and half-life of clearance. Testosterone was used as a positive control. For cytochrome P450 inhibition, CLR01 was prepared at eight concentrations ranging from 0 to 25 μM with each of the following individual human recombinant cytochrome P450 isoforms (1A2, 2C9, 2C19, 2D6 and 3A4) and the appropriate cytochrome P450 substrate. Aliquots of the test samples were extracted using an organic solvent and analysed by high-performance liquid chromatography/mass spectrometry to determine the cytochrome P450 half-maximal inhibition concentration values.

Cytochrome P450 induction by pregnane X receptor reporter gene assay

African green monkey kidney cells were plated in 96-well plates at a density of 7000 cells per well in Dulbecco's modified Eagle medium (Invitrogen) with 10% foetal bovine serum (Fisher Scientific) containing penicillin and streptomycin. Twenty-four hours post-plating, cells were transfected with the appropriate plasmids using Lipofectamine™ 2000 (Invitrogen) according to the manufacturer's instructions. The total DNA per well was 115 ng and contained a mixture of each of the following plasmids: pSV40-β-galactosidase (40 ng), XREM-Luc (20 ng), pSG5-hPXR (5 ng) and pBluescript (50 ng). Luciferase activity was determined using a standard luciferase assay system (Promega). The β-galactosidase activity was determined using standard methods by the *o*-nitrophenolgalactoside assay and was read at 420 nm. Cells were treated with 10 mM rifampicin (Sigma) or CLR01 for 24 h. Data are normalized to β-galactosidase activity (*n* = 8).

Results

CLR01 rescues neurons from amyloid β protein–induced retraction of dendritic spines

The strongest anatomical correlate for the degree of cognitive impairment in Alzheimer's disease is synapse loss (DeKosky and Scheff, 1990; Terry *et al.*, 1991). Post-mortem ultrastructural stereological analysis of the hippocampal CA1 regions of brains
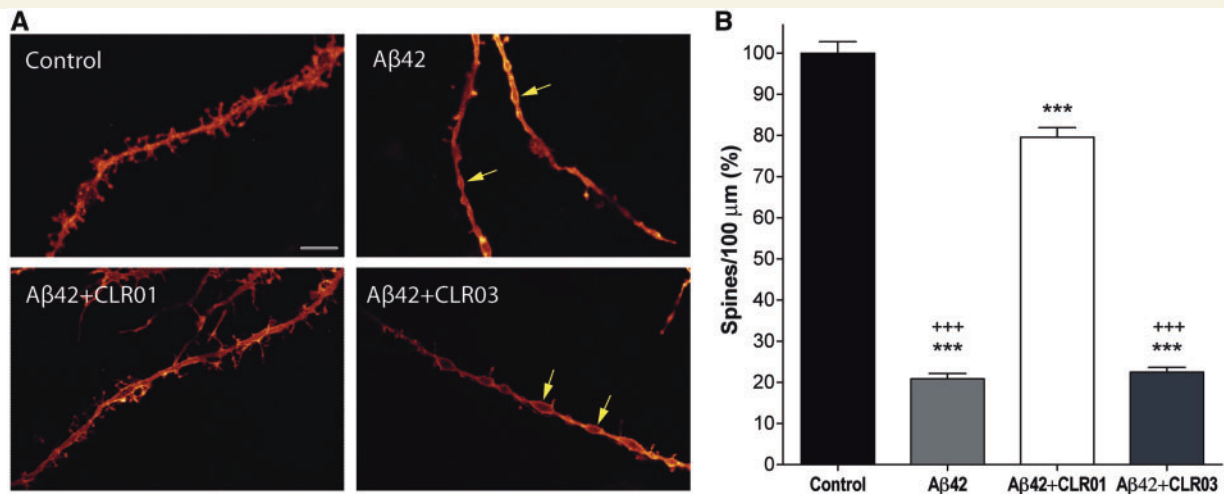
Figure 1 CLR01 protects neurons from amyloid β protein–induced changes in dendritic spine number and morphology. (**A**) Rat primary hippocampal neurons were incubated for 72 h with media alone or with amyloid β_{42} in the absence or presence of molecular tweezers. Yellow arrows point to amyloid β_{42}–induced varicosities. Scale bar = 5 μm. (**B**) The number of dendritic spines per 100 μm was quantified. ***$P < 0.001$ compared with control;$^{+++}P < 0.001$ compared with amyloid β_{42} + CLR01.

of patients with mild cognitive impairment showed 18% synapse loss that progressed to 55% in mild Alzheimer's disease (Scheff et al., 2007). In primary neuronal cultures, oligomers of amyloid β_{42} have been shown to cause substantial decrease in dendritic spine density (Shankar et al., 2008). Additionally, amyloid β toxicity has been shown to lead to neuritic abnormalities and axonal varicosities in Alzheimer's disease mouse models (Tsai et al., 2004; Stokin et al., 2005).

To assess the effect of molecular tweezers on amyloid β_{42}–induced synapse loss, we treated primary hippocampal neurons with 3 μM amyloid β_{42} for 72 h in the presence or absence of 10-fold excess of CLR01 or a negative control derivative, CLR03 (Sinha et al., 2011), and quantified spine density. Amyloid β_{42} induced abundant varicosities (Fig. 1A) and caused a decline in the number of dendritic spines to 20.9% ± 1.3% of baseline (Fig. 1B). In the presence of CLR01, spine density was rescued to 79.6% ± 2.3% of baseline ($P < 0.001$ compared with amyloid β_{42} alone) and varicosities were reduced, whereas CLR03 was inactive (22.5% ± 1.2% of baseline). In these and further experiments addressing synaptotoxicity, we adjusted the amyloid β_{42} concentration empirically to elicit a sufficiently robust toxic response allowing measurement of inhibition by molecular tweezers (see Supplementary material for additional details).

CLR01 prevents disruption of basal synaptic transmission

Changes in gene expression and synaptic vesicle trafficking in the brains of patients with Alzheimer's disease and transgenic mice suggest that synaptic function is compromised before the physical degeneration of the synapses (Westphalen et al., 2003; Yao et al., 2003). Electrophysiological experiments allow measurement of the earliest neuronal insults by amyloid β. Previous reports have documented changes in basal excitatory synaptic neurotransmission

due to amyloid β_{42} deposition (Malinow et al., 2008 and references therein). In a set of experiments designed to test the capability of CLR01 to rescue amyloid β_{42}–induced inhibition of basal synaptic transmission in autaptic microcultures of hippocampal neurons, we measured the amplitudes of excitatory postsynaptic currents, evoked by stimuli mimicking action potentials, in hippocampal neurons exposed for 24 h to 200 nM amyloid β_{42} in the absence or presence of 2 μM CLR01. Culture treatment with amyloid β_{42} alone produced a 51.8% reduction of mean excitatory postsynaptic current amplitude [3.6 ± 0.3 nA ($n = 38$) versus 7.4 ± 0.5 nA in controls ($n = 25$), $P < 0.001$, Fig. 2A]. In contrast, in autaptic hippocampal neurons exposed to amyloid β_{42} in the presence of CLR01 (or with CLR01 alone), excitatory postsynaptic current amplitudes were not significantly different from controls [6.2 ± 0.6 nA ($n = 18$); 6.8 ± 0.7 nA ($n = 18$), respectively].

Application of amyloid β_{42} to hippocampal CA1 pyramidal neurons has been reported to reduce 2-amino-3-(5-methyl-3-oxo-1,2-oxazol-4-yl)propanoic acid receptor-mediated spontaneous miniature excitatory postsynaptic current amplitude and frequency by 60% and 45%, respectively (Parameshwaran et al., 2007). Miniature excitatory postsynaptic current frequency is thought to be a reflection of presynaptic glutamate release, whereas the amplitude reflects the postsynaptic AMPA [2-amino-3-(5-methyl-3-oxo-1,2-oxazol-4-yl)propanoic acid] receptor response to glutamate (Parameshwaran et al., 2007).

Spontaneous neurotransmitter release was studied by recording miniature excitatory postsynaptic current (Fig. 2B) under the same experimental conditions as described earlier. We found that amyloid β_{42} treatment reduced miniature excitatory postsynaptic current amplitude by 34.5% [17.6 ± 1.0 pA ($n = 38$) versus 26.9 ± 1.6 pA in controls ($n = 25$), $P < 0.001$, Fig. 2C] and miniature excitatory postsynaptic current frequency by 41.6% [4.9 ± 0.5 Hz ($n = 38$) versus 8.4 ± 0.8 Hz in control ($n = 25$), $P < 0.005$; Fig. 2D]. In neurons treated with amyloid β_{42} in the
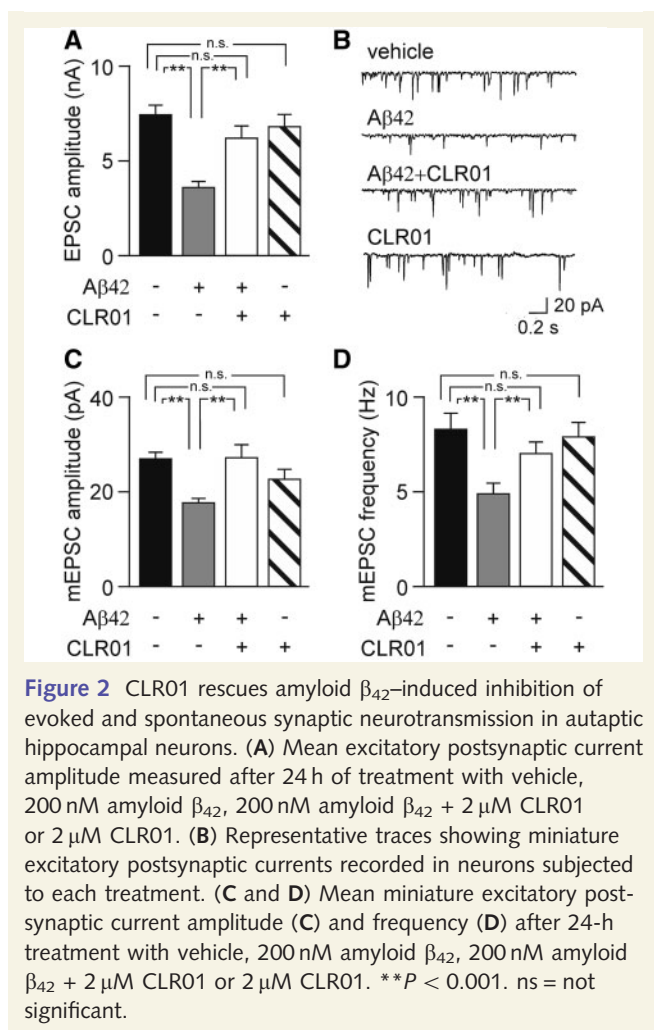
Figure 2 CLR01 rescues amyloid β_{42}–induced inhibition of evoked and spontaneous synaptic neurotransmission in autaptic hippocampal neurons. (**A**) Mean excitatory postsynaptic current amplitude measured after 24 h of treatment with vehicle, 200 nM amyloid β_{42}, 200 nM amyloid β_{42} + 2 μM CLR01 or 2 μM CLR01. (**B**) Representative traces showing miniature excitatory postsynaptic currents recorded in neurons subjected to each treatment. (**C** and **D**) Mean miniature excitatory post-synaptic current amplitude (**C**) and frequency (**D**) after 24-h treatment with vehicle, 200 nM amyloid β_{42}, 200 nM amyloid β_{42} + 2 μM CLR01 or 2 μM CLR01. **P < 0.001. ns = not significant.

presence of CLR01, both parameters were not significantly different from controls [miniature excitatory postsynaptic current amplitude: 27.2 ± 2.7 pA; miniature excitatory postsynaptic current frequency: 7.1 ± 0.6 Hz ($n = 18$)]. Application of CLR01 alone did not significantly affect either the frequency (7.9 ± 0.8 Hz; $n = 18$) or the amplitude (22.5 ± 2.1 pA; $n = 18$) of miniature excitatory postsynaptic current.

CLR01 protects synaptic plasticity against amyloid β_{42}–induced insults

Signalling through AMPA and *N*-methyl-ᴅ-aspartate receptors is critical for long-term potentiation, a cellular correlate for learning and memory that is expressed as an increase in efficiency of synaptic transmission (Bliss and Collingridge, 1993). Inhibition of long-term potentiation, manifested as a decrease in field EPSP amplitudes and slopes, has been observed on application of different amyloid β oligomers to rat hippocampal slices (Lambert *et al.*, 1998; Puzzo *et al.*, 2008).

To further evaluate the protective effect of CLR01 on amyloid β_{42}–induced synaptotoxicity, we studied long-term potentiation at the Schaffer collateral–CA1 synapses in hippocampal brain slices.

The amyloid β concentration selected, 200 nM, did not influence basal synaptic transmission in brain slices, thus avoiding potentially producing confounding effects on long-term potentiation, as documented by the stability of pre-tetanus field EPSP recordings and the absence of significant differences between the pre- and post-amyloid β application input/output curves. Higher amyloid β concentrations (e.g. 500 nM) did inhibit basal synaptic transmission in brain slices (data not shown). Under control conditions, i.e. when hippocampal slices were perfused with vehicle alone for 20 min before high-frequency stimulation, the field EPSP amplitude recorded 60 min post-high-frequency stimulation displayed increases of $+115.0\% \pm 8.8\%$ over baseline ($n = 11$). In hippocampal brain slices perfused with 200 nM amyloid β_{42} for the 20 min preceding high-frequency stimulation, the long-term potentiation was significantly smaller at $+53.7\% \pm 5.1\%$ over baseline ($n = 10$, $P < 0.001$, Fig. 3A). Co-application of 200 nM amyloid β_{42} and 2 μM CLR01 significantly ameliorated long-term potentiation inhibition relative to amyloid β_{42} alone [field EPSP amplitude increases of $+75.4\% \pm 7.7\%$ ($n = 8$), $P < 0.05$, not shown in graph]. Though this rescuing effect was statistically significant, its magnitude was small relative to the protective effects of CLR01 in cell culture (Figs 1 and 2). A potential explanation is differences in diffusion to the cellular targets between amyloid β_{42} oligomers and CLR01, which may diminish the effectiveness of CLR01 in brain slices relative to cultured neurons. To test this hypothesis, we examined whether a 1-h incubation of amyloid β_{42} with CLR01 before application to hippocampal slices would produce stronger protection. Indeed, 1-h preincubation of amyloid β_{42} with CLR01 provided a stronger protective effect, raising the field EPSP amplitude potentiation to $+94.2\% \pm 7.4\%$ over baseline ($n = 12$, $P < 0.001$ versus amyloid β_{42} alone, and $P < 0.05$ versus controls; Fig. 3A and B).

Control long-term potentiation experiments were performed in brain slices exposed to 2 μM CLR01 alone or 200 nM amyloid β_{42} in the presence of 2 μM CLR03. Application of CLR01 alone did not significantly affect long-term potentiation (field EPSP amplitude potentiation of $+113.2\% \pm 11.7\%$ over baseline; $n = 6$), whereas amyloid β_{42} + CLR03 caused long-term potentiation inhibitions not significantly different from those produced by amyloid β_{42} alone ($+53.6\% \pm 5.9\%$; $n = 8$; $P < 0.001$ versus controls, Fig. 3B).

Analysis of the amyloid β_{42} assembly size distribution in the neurobasal media or artificial CSF preparations used in the experiments described previously by native- or SDS-PAGE western blots showed a mixture of species ranging from monomer to large oligomers. Little difference was observed between distributions of species in the absence or presence of molecular tweezers (Supplementary Fig. 1).

CLR01 is pharmacologically stable and penetrates the brain at similar levels in wild-type and transgenic mice

Towards evaluating the potential of molecular tweezers for drug development, we studied the stability of CLR01 in plasma and liver microsomes. Biotransformation of CLR01 was measured during
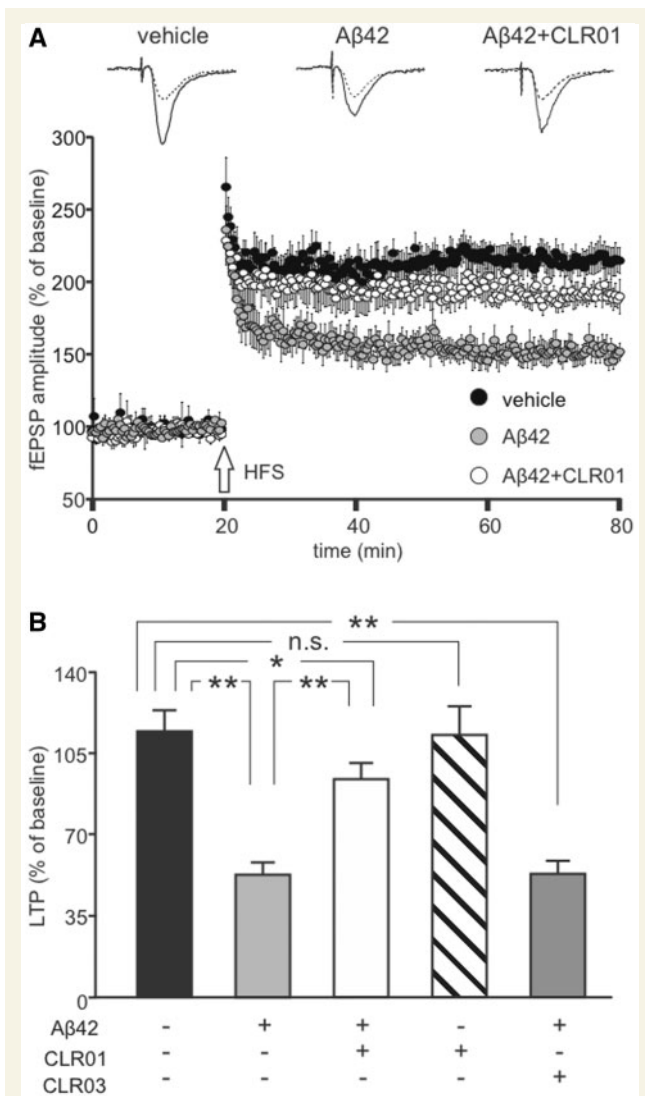
Figure 3 CLR01 attenuates amyloid β$_{42}$–induced inhibition of long-term potentiation (LTP) at CA3–CA1 synapses. (**A**) Time course of field EPSP (fEPSP) amplitudes before and after high-frequency stimulation (HFS) (indicated by arrow) in slices treated for 20 min with vehicle (black circles), 200 nM amyloid β$_{42}$ (grey circles) or 200 nM amyloid β$_{42}$ + 2 µM CLR01 preincubated for 1 h before application (white circles). Results are expressed as percentages of baseline field EPSP amplitude (=100%). Insets show representative traces of field EPSP at baseline (dotted lines) and during the last 5 min of long-term potentiation recording (solid lines). (**B**) Bar graph showing mean long-term potentiation changes measured during the last 5 min of recording after slice exposure to vehicle or different combinations of 200 nM amyloid β$_{42}$, 2 µM CLR01 and 2 µM CLR03. **$P < 0.001$; *$P < 0.05$. ns = not significant.

60-min incubation in human and mouse plasma or liver microsome preparations, an abundant source of drug metabolizing enzymes (Obach *et al.*, 2006; Paine *et al.*, 2006). In comparison with testosterone, which was used as a positive control and was degraded down to 29% in human and 1% in mouse liver microsomes, no degradation of CLR01 was observed in these preparations.

Similarly, CLR01 was found to be 100% stable in human and mouse plasma for 60 min at 37°C.

The blood–brain barrier is suggested to be compromised in humans with Alzheimer's disease (Matsumoto *et al.*, 2007; Zipser *et al.*, 2007) and in transgenic animal models of Alzheimer's disease (Ujiie *et al.*, 2003). Thus, we analysed brain permeability of CLR01 both in triple-transgenic (Oddo *et al.*, 2003) and in healthy wild-type mice to assess how much of the penetration is due to the disruption of the blood–brain barrier seen with disease and how much may be due to other mechanisms, such as transporters. Tritium-labelled CLR01 (^{3}H-CLR01) was administered intravenously to 12-month-old wild-type or triple-transgenic mice. One hour post-injection, blood was collected, mice were perfused to remove blood from the brain vasculature, euthanized and the brains were collected. Brain penetration percentage was calculated as activity per gram of brain relative to activity per millilitre of blood. There was a small non-significant difference in brain penetration of CLR01 between wild-type (1.74% ± 0.35%) and triple-transgenic mice (1.98% ± 0.11%). There was no difference in per cent of injected CLR01 found in the blood 1 h post-injection between wild-type and transgenic mice, 15.5% ± 1.3% and 15.7% ± 3.5%, respectively.

CLR01 reduces brain amyloid β protein and tau burden and ameliorates microgliosis in transgenic mice without apparent toxicity

In light of the promising *in vitro* data, we next conducted an initial *in vivo* study to assess the efficacy of peripherally administered CLR01 in transgenic mice using immunohistochemical changes of amyloid β and p-tau burden, and brain inflammation as endpoints. Similar to the blood–brain barrier experiments described earlier, in these experiments we used the triple-transgenic mouse model of Alzheimer's disease, which overexpresses mutant forms of the human genes encoding presenilin 1 (mutation M146V) and amyloid β protein precursor (mutation KM670/671NL), each of which causes early-onset familial Alzheimer's disease, and tau (mutation P301L), which causes frontotemporal dementia. This mouse model is particularly relevant to pathological features of Alzheimer's disease by encompassing both amyloid plaques and neurofibrillary tangles (Oddo *et al.*, 2003).

Mixed-gender 14–15-month-old mice (*n* = 6–7 per group) were treated for 28 days with 40 µg/kg/d CLR01 in saline as a vehicle, or with vehicle alone, administered subcutaneously using osmotic minipumps. After treatment, the mice were sacrificed and their brains were analysed by immunohistochemistry for the presence of plaques, tangles and inflammatory markers. Analysis of brain sections from vehicle-treated mice using monoclonal antibody 6E10 showed amyloid plaques deposited predominantly in the subiculum and CA1 regions of the hippocampus (Fig. 4A), as reported previously (Oddo *et al.*, 2003). In addition, the mice showed phosphorylated paired helical filaments detected by the anti–p-tau monoclonal antibody AT8, predominantly in the hippocampal regions CA1 and CA3 (Fig. 4D). Mice treated with CLR01 showed a significant decrease in amyloid β burden of 33.3% in
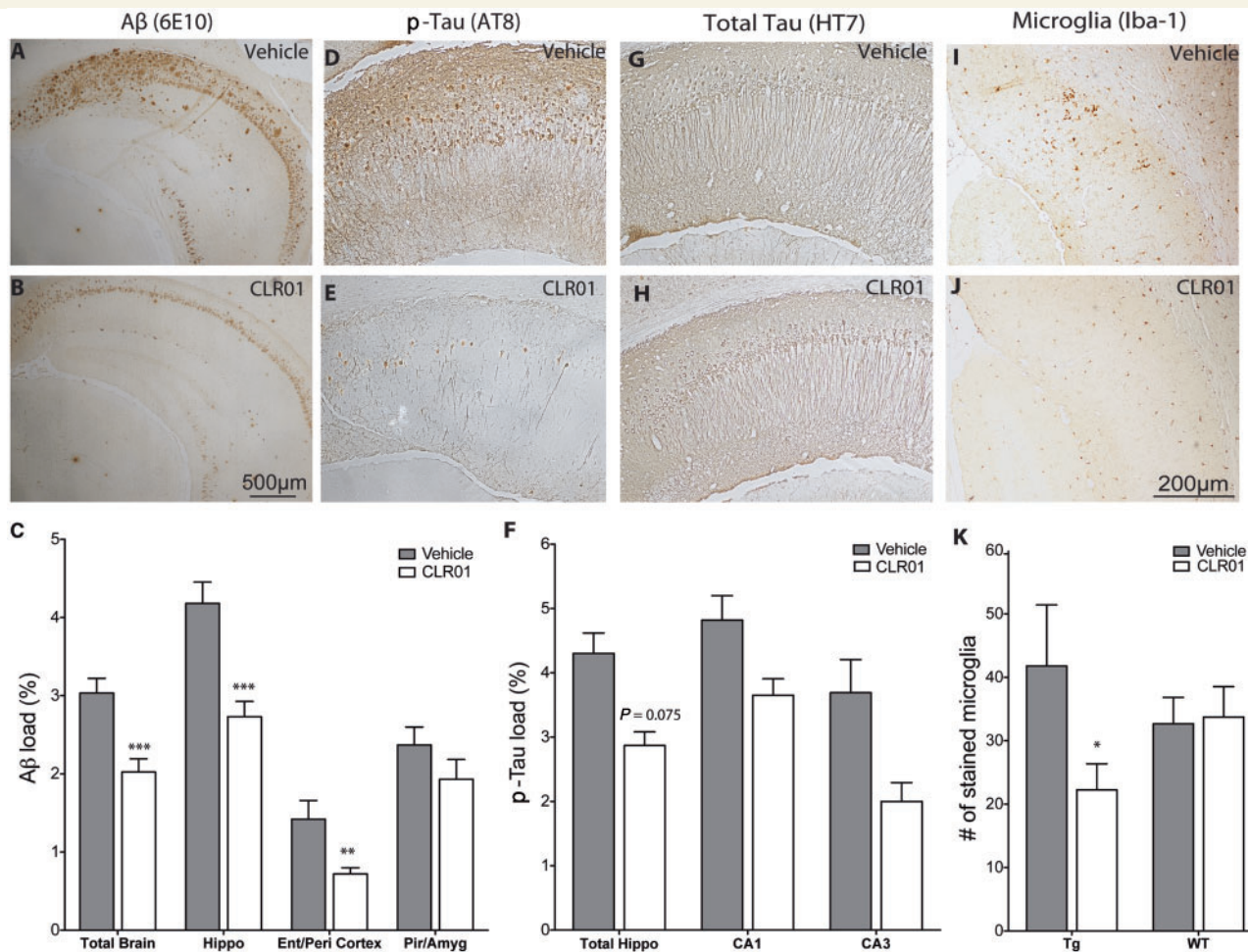
Figure 4 CLR01 decreases amyloid β protein and p-tau deposition and ameliorates microgliosis in transgenic mouse brain. Triple-transgenic mice were treated with 40 μg/kg/d CLR01 or vehicle. (**A, D, G** and **I**) Vehicle-treated transgenic mouse hippocampus. (**B, E, H** and **J**) CLR01-treated transgenic mouse hippocampus. (**A** and **B**) Transgenic mouse brain stained with monoclonal antibody 6E10 showing amyloid plaque deposition. (**C**) Per cent amyloid β (Aβ) burden was quantified by calculating the total 6E10-stained area divided by the total area measured. (**D** and **E**) Transgenic mouse brain showing AT8-positive neurofibrillary tangles in the CA1 region. (**F**) Per cent aggregated p-tau load was quantified by calculating the total AT8-stained area divided by the total area. (**G** and **H**) Transgenic mouse brain stained with monoclonal antibody HT7 for total tau. (**I** and **J**) Transgenic mouse brain showing Iba1-positive microglia in the subiculum and CA1 region. (**K**) Number of stained microglia in a 1.14 mm^2 area of hippocampus per treatment condition. Scale bars: bar in **B** applies to both **A** and **B**; bar in **J** applies to D–J. *$P < 0.05$, **$P < 0.01$, ***$P < 0.001$ compared with vehicle-treated mice. Amyg = amygdala; Ent = entorhinal; Hippo = hippocampus; Peri = perirhinal; Pir = piriform cortices; WT = wild-type.

the total brain area analysed (per cent burden: vehicle-treated 3.03% ± 0.19% versus CLR01-treated 2.02% ± 0.17%, $P < 0.01$, Fig. 4B and C), 34.7% in the hippocampus (vehicle-treated 4.18% ± 0.27% versus CLR01-treated 2.73% ± 0.20%, $P < 0.05$), 49.3% in the perirhinal and entorhinal cortices (vehicle-treated 1.42% ± 0.24% versus CLR01-treated 0.72% ± 0.08%, $P < 0.05$) and 18.6% in the piriform cortex and amygdala (vehicle-treated 2.37% ± 0.23% versus CLR01-treated 1.93% ± 0.25%). Similarly, a 33.3% reduction in AT8-positive p-tau was observed in the total brain area analysed (% burden: vehicle-treated 4.30% ± 0.32% versus CLR01-treated 2.87% ± 0.21%, Fig. 4E and F), 24.3% reduction in CA1 (vehicle-treated 4.82% ± 0.38% versus CLR01-treated 3.65% ± 0.26%) and a 45.8% reduction in CA3 (vehicle-treated

3.69% ± 0.52% versus CLR01-treated 2.00% ± 0.29%) regions in mice treated with CLR01. In contrast, immunohistochemistry with the anti-tau monoclonal antibody HT7 showed no effect on total tau (Fig. 4G and H).

Compared with vehicle-treated triple-transgenic mice (Fig. 4I), the CLR01-treated triple-transgenic mice showed a 46.2% reduction in the number of microglia per hippocampal area (vehicle-treated 41.79 ± 9.64 versus CLR01-treated 22.5 ± 4.12, $P < 0.05$; Fig. 4J and K) and in the microglial stained area (data not shown). Similarly, a 43.9% reduction in microglial stained area was found in the cortex of CLR01-treated mice relative to vehicle-treated mice (data not shown). In comparison, there was essentially no difference between vehicle- and CLR01-treated wild-type mice in the level of microgliosis (vehicle-treated

32.67 ± 4.16 versus CLR01-treated 33.73 ± 4.81, Fig. 4K). In contrast to the effect on microglia, CLR01 treatment had little or no impact on the number or staining level of astrocytes in transgenic or wild-type mice in either the hippocampus or cortex (data not shown).

As has been described previously (Hirata-Fukae et al., 2008), we found that the triple-transgenic female mice in our study had more amyloid β pathology than the males. The vehicle-treated females ($n = 3$) had 204% the amyloid β load of the males ($n = 3$) in the hippocampus, 394% in the entorhinal/perirhinal cortices and 205% in the piriform cortex/amygdala region. A similar trend was observed with the CLR01-treated mice ($n = 4$ females, 3 males): 138% in the hippocampus, 164% in the entorhinal/perirhinal cortices and 308% in the piriform cortex/amygdala region. Correspondingly the effect of CLR01 treatment was substantially more pronounced in females than in males. Female mice showed a decrease of 45% in amyloid β load in the hippocampus, whereas males had a decrease of 19%. A similar trend was observed in the entorhinal/perirhinal cortices, 64% decrease in females and 15% decrease in males, whereas in the piriform cortex/amygdala region, the trend was reversed—17% decrease in females and a 45% decrease in males. Consistent with the previous study (Hirata-Fukae et al., 2008), the p-tau load did not differ significantly between male and female triple-transgenic vehicle-treated mice, and CLR01 treatment affected p-tau load to the same extent in both genders.

Because CLR01 may bind to Lys residues in proteins other than amyloid β and tau and affect their activity, we used several criteria, including appetite loss, weight loss (Table 1), lethargy and mortality to explore whether CLR01 treatment had adverse effects on the triple-transgenic mice. We did not observe any adverse effects. To assess potential interactions between CLR01 treatment and general behavioural measures, mouse activity was analysed during a single 7-min monitoring period. We did not observe any significant changes in velocity, path shape or mobility between the CLR01-treated and the vehicle-treated transgenic or wild-type mice (Table 2). Similarly, no effects were observed on habituation rates in any of these measures (Table 2). As hyperactivity and other perturbations of locomotor activity, as well as disruptions of habituation, have commonly been observed after CNS toxicity (Platel and Porsolt, 1982; Hess et al., 1986), the lack of such behavioural effects suggests that the 28-day CLR01 regimen did not adversely impact the neural systems subserving these traits.

To address further potential concerns regarding toxicity due to the unique mechanism of CLR01, we studied the effect of CLR01 in several in vitro and in vivo systems. Previously, CLR01 showed no toxicity at $<400\,\mu M$ in cell lines and in primary neurons (Sinha et al., 2011, 2012a), a concentration that is 1–3 orders of magnitude higher than needed for inhibition of toxicity in cell culture. Zebrafish treated with CLR01 up to $10\,\mu M$ dissolved in the water in which the fish developed showed no signs of toxicity (Prabhudesai et al., 2012). In mouse brain slices treated with $2\,\mu M$ CLR01 alone, no changes were seen in levels of long-term potentiation (Fig. 3B). We also did not find adverse effects by weight, activity or mortality in mice treated subcutaneously with CLR01 doses from $40\,\mu g/kg/d$ (Tables 1 and 2) up to $1200\,\mu g/kg/d$ (data not shown) or in mice treated intracerebroventricularly with $10\,\mu M$ CLR01 (data not shown), suggesting the existence of sufficient therapeutic window for CLR01. Further, we assessed the effect of CLR01 on amyloid β protein precursor processing. In the amyloid β protein precursor sequence, Lys residues exist directly N-terminal to the α-secretase cleavage site and two residues N-terminal to the β-secretase cleavage site (in the triple-transgenic

Table 1 No toxic effect of CLR01 on weight change (% of pre-surgery baseline)

Genotype	Treatment	Day 0	Day 8	Day 23	Day 28
Wild-type	Vehicle	100.0 ± 0.0	96.7 ± 0.01	97.8 ± 0.01	96.2 ± 0.01
	CLR01	100.0 ± 0.0	95.6 ± 0.05	96.2 ± 0.01	95.8 ± 0.01
Triple-transgenic	Vehicle	100.0 ± 0.0	95.6 ± 0.02	97.4 ± 0.01	97.6 ± 0.02
	CLR01	100.0 ± 0.0	95.9 ± 0.02	100.4 ± 0.02	97.8 ± 0.03

Table 2 No toxicity of CLR01 by behavioural end-points

Genotype	Treatment	Velocity (cm/s)	Velocity habituation (% change)	Mobility (% time)	Mobility habituation (% change)	Meander (°/cm)	Meander habituation (% change)
Wild-type	Vehicle	4.6 ± 0.6	-24 ± 7	63 ± 6	-33 ± 13	425 ± 39	40 ± 10
	CLR01	5 ± 1	-15 ± 16	65 ± 5	-50 ± 31	418 ± 34	48 ± 20
Triple-transgenic	Vehicle	5.5 ± 0.7	-24 ± 8	71 ± 4	-25 ± 11	377 ± 32	49 ± 15
	CLR01	5.6 ± 0.7	-9 ± 7	75 ± 4	-8 ± 6	358 ± 30	21 ± 8
P-value (two-way ANOVA)	Treatment effect	0.62	0.23	0.58	0.99	0.71	0.49
	Genotype effect	0.43	0.77	0.083	0.19	0.12	0.52
	Interaction effect	0.78	0.80	0.82	0.35	0.85	0.21

mice we used here, the Lys–Met dipeptide at positions 670 and 671 is replaced by Asn–Leu). Additionally, several Lys residues are a few amino acids C-terminal to the γ-secretase cleavage site. Brain extracts from wild-type and transgenic mice treated with either vehicle or CLR01 were analysed by Western blots using antibodies specific for the soluble N-terminal portion of amyloid β protein precursor, or for the C-terminal fragments of amyloid β protein precursor. We found no differences in concentration levels of soluble amyloid β protein precursor, C-terminal fragment-α or C-terminal fragment-β between vehicle- and CLR01-treated mice (Supplementary Fig. 2), supporting CLR01's putative process-specific mechanism of action.

CLR01 interacts weakly with major cytochrome P450 isoforms

The cytochrome P450 family of enzymes catalyses the oxidation of a vast array of endobiotic and xenobiotic molecules to increase their hydrophilicity during phase-I metabolism, accounting for ~75% of the total number of metabolic reactions in the body (Williams *et al.*, 2004; Guengerich, 2008). Thus, inhibition or activation of cytochrome P450 enzymes may cause metabolic toxicity. In addition, drug–drug interactions are an important consideration in the development of new therapeutics and are highly related to the cytochrome P450 system. Induction or inhibition of particular cytochrome P450 isozymes by one drug or food product may affect the rate of metabolism of other substrates (i.e. drugs) of these isozymes. Thus, it is important to evaluate the interaction of molecular tweezers with cytochrome P450 if they are to become drug candidates.

Measurement of the inhibitory potency of CLR01 on five major cytochrome P450 isoforms responsible for 95% of drug metabolism (Williams *et al.*, 2004) yielded the following half-maximal inhibition concentration values, listed in order from the most potently inhibited enzyme to the least: 2C19 (1.5 μM) > 3A4

(1.7 μM) > 2C9 (2.2 μM) > 2D6 (3.6 μM) > 1A2 (>20 μM). Inhibitory potency values <1 μM are expected to cause drug interactions of at least 2-fold, based on comparison of *in vivo* drug interaction data and primary experimental *in vitro* results for 44 drugs (Obach *et al.*, 2006). The half-maximal inhibition concentration values for the interaction of CLR01 with cytochrome P450 were above the 1-μM threshold for all the isoforms tested. The *in vitro* inhibition order is generally expected to line up with the *in vivo* magnitude of drug–drug interactions involving the substrates for the specific cytochrome P450 isoforms (Obach *et al.*, 2006).

We also evaluated induction of the cytochrome P450 system using the pregnane X receptor (PXR) reporter gene assay (Jones *et al.*, 2002). PXR is a nuclear receptor and transcription factor for genes that are highly involved in xenobiotic and endobiotic uptake, metabolism and elimination. It is a key activator of the xenobiotic-inducible cytochrome P450 isoforms 3A, 2B, and 2C and of glutathione S-transferase gene expression. Importantly, the PXR ligand-binding domain is uniquely large allowing the receptor to bind promiscuously to a large variety of structurally diverse molecules in different orientations (Staudinger *et al.*, 2006), making it a robust target whose activation can be used to predict cytochrome P450 induction and potential toxicity of new experimental drugs (Staudinger and Lichti, 2008).

To evaluate PXR activation and potential toxicity of CLR01, African green monkey kidney fibroblasts were transfected with plasmids containing luciferase and β-galactosidase reporter genes under control of a PXR response element. Forty-eight hours post-transfection, the cells were treated for 24 h with 10 μM rifampicin, an antibiotic and known PXR ligand, as a positive control, or with different concentrations of CLR01. At concentrations up to 1 μM, CLR01 exhibited luciferase activity similar to that of vehicle alone. At 10 and 50 μM, CLR01 induced a luciferase activity 56.4% and 39.5% the magnitude of rifampicin, respectively (Fig. 5). CLR01 (50 μM) reduced the β-galactosidase
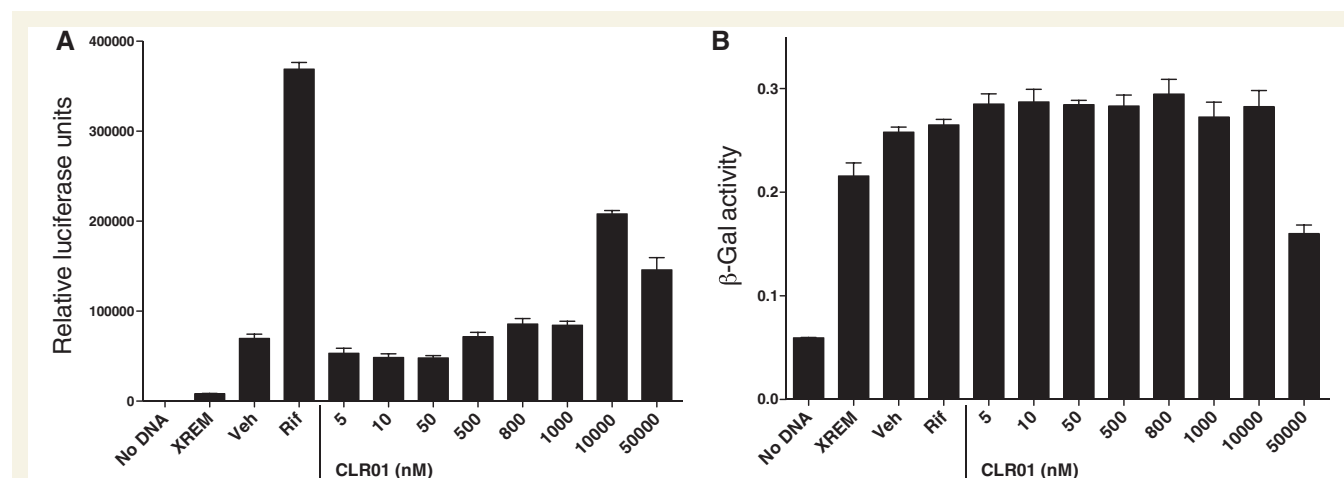

Figure 5 Weak induction of the cytochrome P450 system by CLR01. African green monkey kidney cells were treated with 10 μM rifampicin (rif; positive control) or CLR01 for 24 h. Cells transfected with luciferase but not PXR (XREM) were used as a negative control. (**A**) Luciferase activity was determined using a standard luciferase assay system (Promega). (**B**) β-galactosidase activity was determined using standard methods by the *o*-nitrophenolgalactoside assay.

induction by 39.6%. These data demonstrate minimal PXR activation by low micromolar concentrations of CLR01 compared with a known ligand of PXR and a commonly used drug, rifampicin.

The highest plasma concentration found in pharmacokinetic experiments in which CLR01 was administered intravenously at 1 mg/kg (25 times the dose used for the experiments shown in Fig. 4) was $< 11 \mu M$ at time zero, suggesting that toxicity is not anticipated at doses needed for the *in vivo* effects observed on aggregated amyloid β, p-tau and microgliosis.

Discussion

We have recently reported that CLR01 is a process-specific inhibitor of aberrant assembly and toxicity of amyloidogenic proteins (Sinha *et al.*, 2011). The putative mechanism of action of molecular tweezers and the reason we refer to them as process-specific is their labile moderate-affinity binding to solvent-exposed Lys residues, thereby disrupting a combination of hydrophobic and electrostatic interactions that are key to the aberrant self-assembly process. We previously showed that CLR01 inhibited the assembly and toxicity of multiple disease-associated proteins, disaggregated preformed amyloid β fibrils and stabilized non-toxic assemblies (Sinha *et al.*, 2011). Additionally, by a similar effect on α-synuclein, CLR01 prevented developmental deformities and death and facilitated proteasomal clearance of α-synuclein in a novel zebrafish model (Prabhudesai *et al.*, 2012). Following up on these promising efficacy data and minimal toxicity found for CLR01 in cell culture or in zebrafish, here we report its capability to protect synaptic structure, function and plasticity against amyloid β insults and to ameliorate brain pathology in Alzheimer's disease transgenic mice.

Based on *in vitro* experiments using electron microscopy, dot blots with an oligomer-specific antibody, dynamic light scattering and solution-state nuclear magnetic resonance (Sinha *et al.*, 2011), we expected that incubation of amyloid β_{42} with CLR01 would lead to a rapid modulation of amyloid β_{42} to a non-toxic state. Using electrophysiological readouts as functional correlates of the toxicity state, we found that CLR01 provided significant relief from amyloid β_{42}–induced toxic effects on basal synaptic activity and long-term potentiation, supporting our prediction. Additionally, comparison of co-application with preincubation of amyloid β and CLR01 before addition to brain slices in long-term potentiation experiments showed that preincubation increased the protective effect without changing the distribution of amyloid β species as analysed by native- and SDS-PAGE western blots (Supplementary Fig. 1). The lack of difference seen by the Western blot analysis compared with the positive difference seen in cell viability (Sinha *et al.*, 2011, 2012a), dendritic spine (Fig. 1) and electrophysiological assays (Figs 2 and 3) suggest that the changes in amyloid β assembly induced by CLR01 are subtle or that CLR01 binding prevents contact with the cellular targets of the toxic amyloid β species. The increased protective effect after preincubation supports our previous findings of rapid disruption of amyloid β_{42} self-association and its remodelling into non-toxic structures by CLR01 (Sinha *et al.*, 2011), which is common to a number of inhibitors (Liu and Bitan, 2012). One such inhibitor,

scyllo-inositol, was shown to inhibit long-term potentiation deficits caused by cell-secreted amyloid β oligomers when preincubated with conditioned media containing these oligomers before application to slices (Townsend *et al.*, 2006), similar to CLR01, whereas post-application of *scyllo*-inositol after incubation of cells with the conditioned media provided no protection against amyloid β toxicity. Additional comparison of our electrophysiological data with previous literature is provided in the Supplementary material.

As a first step in characterizing CLR01 *in vivo*, we quantified the blood–brain barrier permeability of CLR01 in both wild-type and transgenic mice. Though blood–brain barrier disruption has been reported in Alzheimer's disease and transgenic mouse models, we found genotype-independent ~2% blood–brain barrier permeability, 1 h post-injection, in both 12-month-old wild-type and triple-transgenic mice, consistent with a previous study of the triple-transgenic mice at 11-months of age (Bourasset *et al.*, 2009). At this age range, the mice display a moderate disease phenotype, which apparently does not affect blood–brain barrier integrity.

Next, we assessed brain amyloid β and p-tau load in a small group of transgenic mice treated continuously for 28 days and found a significant decrease in amyloid β levels (Fig 4). Similar effects were observed on p-tau and microglia, however, because of the small sample size, statistical significance was not reached in all cases. Based on CLR01's ability to disaggregate preformed fibrils *in vitro* (Sinha *et al.*, 2011), it is possible that a similar action disaggregated amyloid plaques in the brains of the treated mice into soluble non-toxic structures amenable to clearance and/ or degradation. Although additional experiments are needed to establish the mechanism by which CLR01 exerted its beneficial effects in the mice, the clearance hypothesis is supported by our recent *in vivo* study in zebrafish expressing human α-synuclein that were treated with CLR01 and showed recovery of proteasomal activity and increased α-synuclein clearance (Prabhudesai *et al.*, 2012).

Consistent with amyloid β–induced neuroinflammation (Akiyama *et al.*, 2000), the reduction in amyloid β load correlated with a decrease in microgliosis (Fig. 4). Although activation of microglia plays a dual role in the brain, phagocytosing deposited amyloid β (Frautschy *et al.*, 1992; Ard *et al.*, 1996) and releasing cytotoxic compounds, such as reactive oxygen and nitrogen species (Colton and Gilbert, 1987; Chao *et al.*, 1992), reducing brain microgliosis is typically considered a beneficial treatment outcome in Alzheimer's disease (Akiyama *et al.*, 2000).

Although mechanisms of tau toxicity in Alzheimer's disease are still under discussion, oligomerization and hyperphosphorylation, likely downstream of amyloid β insults, are believed to be involved (Bloom *et al.*, 2005; Gendron and Petrucelli, 2009). We found reduction in levels of p-tau (Fig. 4), which could result from either direct disaggregation by CLR01 as was shown *in vitro* (Sinha *et al.*, 2011) and eventual clearance downstream of the significant decrease in amyloid β aggregates, or reflect both mechanisms. Answering this question will require additional exploration, yet the data suggest that molecular tweezers' process-specific mode of action is uniquely suitable to affect both the amyloid β and tau components of Alzheimer's disease

pathology, and therefore using these compounds is a promising intervention strategy.

Labile binding to Lys residues with micromolar affinity is a unique mode of action that potentially could disrupt normal protein function and cause side effects. However, the aberrant self-assembly process that leads to the formation of toxic amyloid β and tau oligomers involves many weak intra- and intermolecular interactions (Roberts and Shorter, 2008). Thus, the labile binding of molecular tweezers is predicted to be effective in preventing these weak interactions without substantially disrupting structurally stable proteins. In practice, solvent-exposed Lys residues are commonly used for covalent attachment of biotin, fluorescent dyes or other tags without interfering with biological activity of stably folded proteins. It is therefore plausible that non-covalent binding of CLR01 to these proteins with high on–off rate does not affect their bioactivity. Supporting this proposed process-specific mechanism, we found no interference with amyloid β protein precursor processing (Supplementary Fig. 2) despite the proximity of Lys residues to both the α- and β-secretase cleavage sites in wild-type amyloid precursor protein (α-secretase only in the triple-transgenic mice). Similarly, we showed previously that the labile binding of CLR01 to Lys residues prevented α-synuclein aggregation but not the ubiquitination required for proteasomal clearance (Prabhudesai *et al.*, 2012).

Because synaptic deterioration before neuronal loss correlates with onset of amnestic mild cognitive impairment (Arendt, 2009), it can be considered a prominent pathological feature of Alzheimer's disease. Thus, treatments that can prevent the loss of functional synapses during prodromal or early stages of the disease may complement the brain's innate compensatory defence mechanisms and significantly forestall additional Alzheimer's disease-related cognitive symptoms. Furthermore, structural and functional synaptic alterations have been shown to be pharmacologically reversible in old, transgenic mice with Alzheimer's disease (Smith *et al.*, 2009), suggesting that treatment after minor synaptic loss, but before overt neuronal loss, might delay or even reverse cognitive dysfunction. The prevention of spine retraction (Fig. 1), rescue of amyloid β-induced reduction in basal synaptic activity (Fig. 2) and improvement of long-term potentiation (Fig. 3) by CLR01 demonstrate its ability to ameliorate Alzheimer's disease-associated phenotypes of synaptic dysfunction.

Process-specific modulation of amyloid protein self-assembly is a novel approach towards treatment of amyloidoses. Much work still lies ahead for developing molecular tweezers as therapeutic tools for amyloid-related disease, including addressing additional questions about potential toxicity in more stringent systems and therapeutic effects on disease-associated behavioural deficits. As multiple proteins of unrelated sequences cause amyloidoses, a treatment paradigm that is process-specific is a promising approach to the problem. With brain penetration of ∼2% of blood levels, robust stability in plasma and liver microsomes, and weak interaction with major cytochrome P450 isoforms, CLR01 shows a favourable drug profile and is expected to be stable inside the brain. Development of pro-drug derivatives and/or formulations of CLR01 will likely improve further the compound's pharmacokinetic/pharmacodynamic characteristics and increase the likelihood of it becoming a viable drug candidate.

Supplementary material

Supplementary material is available at *Brain* online.

References

Thies W, Bleiler L. Alzheimer's Association 2011 Alzheimer's disease facts and figures. Alzheimers Dement 2011; 7: 208–44.

Abramoff MD, Magelhaes PJ, Ram SJ. Image processing with ImageJ. Biophotonics Intl 2004; 11: 36–42.

Akiyama H, Barger S, Barnum S, Bradt B, Bauer J, Cole GM, et al. Inflammation and Alzheimer's disease. Neurobiol Aging 2000; 21: 383–421.

Ard MD, Cole GM, Wei J, Mehrle AP, Fratkin JD. Scavenging of Alzheimers amyloid β-protein by microglia in culture. J Neurosci Res 1996; 43: 190–202.

Arendt T. Synaptic degeneration in Alzheimer's disease. Acta Neuropathol 2009; 118: 167–79.

Bliss TV, Collingridge GL. A synaptic model of memory: long-term potentiation in the hippocampus. Nature 1993; 361: 31–39.

Bloom GS, Ren K, Glabe CG. Cultured cell and transgenic mouse models for tau pathology linked to β-amyloid. Biochim Biophys Acta 2005; 1739: 116–24.

Bourasset F, Ouellet M, Tremblay C, Julien C, Do TM, Oddo S, et al. Reduction of the cerebrovascular volume in a transgenic mouse model of Alzheimer's disease. Neuropharmacology 2009; 56: 808–13.

Buxbaum JD, Gandy SE, Cicchetti P, Ehrlich ME, Czernik AJ, Fracasso RP, et al. Processing of Alzheimer β/A4 amyloid precursor protein: modulation by agents that regulate protein phosphorylation. Proc Natl Acad Sci USA 1990; 87: 6003–6.

Chao CC, Hu S, Molitor TW, Shaskan EG, Peterson PK. Activated microglia mediate neuronal cell injury via a nitric oxide mechanism. J Immunol 1992; 149: 2736–41.

Cohen TJ, Guo JL, Hurtado DE, Kwong LK, Mills IP, Trojanowski JQ, et al. The acetylation of tau inhibits its function and promotes pathological tau aggregation. Nat Commun 2011; 2: 252.

Colton CA, Gilbert DL. Production of superoxide anions by a CNS macrophage, the microglia. FEBS Lett 1987; 223: 284–8.

DeKosky ST, Scheff SW. Synapse loss in frontal cortex biopsies in Alzheimer's disease: correlation with cognitive severity. Ann Neurol 1990; 27: 457–64.

Fokkens M, Schrader T, Klärner FG. A molecular tweezer for lysine and arginine. J Am Chem Soc 2005; 127: 14415–21.

Frautschy SA, Cole GM, Baird A. Phagocytosis and deposition of vascular β-amyloid in rat brains injected with Alzheimer β-amyloid. Am J Pathol 1992; 140: 1389–99.

Frautschy SA, Hu W, Kim P, Miller SA, Chu T, Harris-White ME, et al. Phenolic anti-inflammatory antioxidant reversal of Aβ-induced cognitive deficits and neuropathology. Neurobiol Aging 2001; 22: 993–1005.

Fusco S, Ripoli C, Podda MV, Ranieri SC, Leone L, Toietta G, et al. A role for neuronal cAMP responsive-element binding (CREB)-1 in brain responses to calorie restriction. Proc Natl Acad Sci USA 2012; 109: 621–6.

Gale GD, Yazdi RD, Khan AH, Lusis AJ, Davis RC, Smith DJ. A genome-wide panel of congenic mice reveals widespread epistasis of behavior quantitative trait loci. Mol Psychiatry 2009; 14: 631–45.

Gendron TF, Petrucelli L. The role of tau in neurodegeneration. Mol Neurodegener 2009; 4: 13.

Guengerich FP. Cytochrome p450 and chemical toxicology. Chem Res Toxicol 2008; 21: 70–83.

Hess EJ, Albers LJ, Le H, Creese I. Effects of chronic SCH23390 treatment on the biochemical and behavioral properties of D1 and D2 dopamine receptors: potentiated behavioral responses to a D2 dopamine agonist after selective D1 dopamine receptor upregulation. J Pharmacol Exp Ther 1986; 238: 846–54.

Hirata-Fukae C, Li HF, Hoe HS, Gray AJ, Minami SS, Hamada K, et al. Females exhibit more extensive amyloid, but not tau, pathology in an Alzheimer transgenic model. Brain Res 2008; 1216: 92–103.

Huang A, Stultz CM. The effect of a ΔK280 mutation on the unfolded state of a microtubule-binding repeat in Tau. PLoS Comput Biol 2008; 4: e1000155.

Jones SA, Moore LB, Wisely GB, Kliewer SA. Use of in vitro pregnane X receptor assays to assess CYP3A4 induction potential of drug candidates. Methods Enzymol 2002; 357: 161–70.

Kayed R. Anti-tau oligomers passive vaccination for the treatment of Alzheimer's disease. Hum Vaccin 2010; 6: 47–51.

Kirkitadze MD, Bitan G, Teplow DB. Paradigm shifts in Alzheimer's disease and other neurodegenerative disorders: the emerging role of oligomeric assemblies. J Neurosci Res 2002; 69: 567–77.

Lambert MP, Barlow AK, Chromy BA, Edwards C, Freed R, Liosatos M, et al. Diffusible, nonfibrillar ligands derived from Aβ$_{1-42}$ are potent central nervous system neurotoxins. Proc Natl Acad Sci USA 1998; 95: 6448–53.

Lazo ND, Grant MA, Condron MC, Rigby AC, Teplow DB. On the nucleation of amyloid β-protein monomer folding. Protein Sci 2005; 14: 1581–96.

Li W, Sperry JB, Crowe A, Trojanowski JQ, Smith AB 3rd, Lee VM. Inhibition of tau fibrillization by oleocanthal via reaction with the amino groups of tau. J Neurochem 2009; 110: 1339–51.

Lim GP, Yang F, Chu T, Chen P, Beech W, Teter B, et al. Ibuprofen suppresses plaque pathology and inflammation in a mouse model for Alzheimer's disease. J Neurosci 2000; 20: 5709–14.

Liu T, Bitan G. Modulating self-assembly of amyloidogenic proteins as a therapeutic approach for neurodegenerative diseases: strategies and mechanisms. ChemMedChem 2012; 7: 359–74.

Maiti P, Piacentini R, Ripoli C, Grassi C, Bitan G. Surprising toxicity and assembly behaviour of amyloid β-protein oxidized to sulfone. Biochem J 2010; 433: 323–32.

Malinow R, Hsieh H, Wei W. Impact of β amyloid on excitatory synaptic transmission and plasticity. In: Synaptic plasticity and the mechanism of Alzheimer's disease. Berlin, Heidelberg: Springer-Verlag; 2008. p. 63–8.

Matsumoto Y, Yanase D, Noguchi-Shinohara M, Ono K, Yoshita M, Yamada M. Blood-brain barrier permeability correlates with medial temporal lobe atrophy but not with amyloid-β protein transport across the blood-brain barrier in Alzheimer's disease. Dement Geriatr Cogn Disord 2007; 23: 241–5.

Obach RS, Walsky RL, Venkatakrishnan K, Gaman EA, Houston JB, Tremaine LM. The utility of in vitro cytochrome P450 inhibition data

in the prediction of drug-drug interactions. J Pharmacol Exp Ther 2006; 316: 336–48.

Oddo S, Caccamo A, Shepherd JD, Murphy MP, Golde TE, Kayed R, et al. Triple-transgenic model of Alzheimer's disease with plaques and tangles: intracellular Aβ and synaptic dysfunction. Neuron 2003; 39: 409–21.

Paine MF, Hart HL, Ludington SS, Haining RL, Rettie AE, Zeldin DC. The human intestinal cytochrome P450 "pie". Drug Metab Dispos 2006; 34: 880–6.

Parameshwaran K, Sims C, Kanju P, Vaithianathan T, Shonesy BC, Dhanasekaran M, et al. Amyloid β-peptide Aβ(1-42) but not Aβ(1-40) attenuates synaptic AMPA receptor function. Synapse 2007; 61: 367–74.

Petkova AT, Ishii Y, Balbach JJ, Antzutkin ON, Leapman RD, Delaglio F, et al. A structural model for Alzheimer's β-amyloid fibrils based on experimental constraints from solid state NMR. Proc Natl Acad Sci USA 2002; 99: 16742–7.

Platel A, Porsolt RD. Habituation of exploratory activity in mice: a screening test for memory enhancing drugs. Psychopharmacology (Berl) 1982; 78: 346–52.

Prabhudesai S, Sinha S, Attar A, Kotagiri A, Fitzmaurice AG, Lakshmanan R, et al. A novel "Molecular Tweezer" inhibitor of α-synuclein neurotoxicity in vitro and in vivo. Neurotherapeutics 2012; 9: 464–76.

Puzzo D, Privitera L, Leznik E, Fa M, Staniszewski A, Palmeri A, et al. Picomolar amyloid-β positively modulates synaptic plasticity and memory in hippocampus. J Neurosci 2008; 28: 14537–45.

Rahimi F, Maiti P, Bitan G. Photo-induced cross-linking of unmodified proteins (PICUP) applied to amyloidogenic peptides. J Vis Exp 2009. http://www.jove.com/index/details.stp?id=1071.

Ripoli C, Piacentini R, Riccardi E, Leone L, Li Puma DD, Bitan G, et al. Effects of different amyloid β-protein analogues on synaptic function. Neurobiol Aging 2012.

Roberts BE, Shorter J. Escaping amyloid fate. Nat Struct Mol Biol 2008; 15: 544–6.

Scheff SW, Price DA, Schmitt FA, DeKosky ST, Mufson EJ. Synaptic alterations in CA1 in mild Alzheimer disease and mild cognitive impairment. Neurology 2007; 68: 1501–8.

Shankar GM, Li S, Mehta TH, Garcia-Munoz A, Shepardson NE, Smith I, Brett FM, et al. Amyloid-β protein dimers isolated directly from Alzheimer's brains impair synaptic plasticity and memory. Nat Med 2008; 14: 837–42.

Sinha S, Du Z, Maiti P, Klärner F-G, Schrader T, Wang C, et al. Comparison of three amyloid assembly inhibitors – the sugar scyllo-inositol, the polyphenol epigallocatechin gallate, and the molecular tweezer CLR01. ACS Chem Neurosci 2012a; 3: 451–458.

Sinha S, Lopes DH, Du Z, Pang ES, Shanmugam A, Lomakin A, et al. Lysine-specific molecular tweezers are broad-spectrum inhibitors of assembly and toxicity of amyloid proteins. J Am Chem Soc 2011; 133: 16958–69.

Sinha S, Lopes DHJ, Bitan G. A key role for lysine residues in amyloid β-protein folding, assembly, and toxicity. ACS Chem Neurosci 2012b; 3: 473–81.

Smith DL, Pozueta J, Gong B, Arancio O, Shelanski M. Reversal of long-term dendritic spine alterations in Alzheimer disease models. Proc Natl Acad Sci USA 2009; 106: 16877–82.

Staudinger JL, Ding X, Lichti K. Pregnane X receptor and natural products: beyond drug-drug interactions. Expert Opin Drug Metab Toxicol 2006; 2: 847–57.

Staudinger JL, Lichti K. Cell signaling and nuclear receptors: new opportunities for molecular pharmaceuticals in liver disease. Mol Pharm 2008; 5: 17–34.

Stokin GB, Lillo C, Falzone TL, Brusch RG, Rockenstein E, Mount SL, et al. Axonopathy and transport deficits early in the pathogenesis of Alzheimer's disease. Science 2005; 307: 1282–8.

Talbiersky P, Bastkowski F, Klärner FG, Schrader T. Molecular clip and tweezer introduce new mechanisms of enzyme inhibition. J Am Chem Soc 2008; 130: 9824–8.

Terry RD, Masliah E, Salmon DP, Butters N, DeTeresa R, Hill R, et al. Physical basis of cognitive alterations in Alzheimer's disease: synapse loss is the major correlate of cognitive impairment. Ann Neurol 1991; 30: 572–80.

Townsend M, Cleary JP, Mehta T, Hofmeister J, Lesné S, O'Hare E, et al. Orally available compound prevents deficits in memory caused by the Alzheimer amyloid-β oligomers. Ann Neurol 2006; 60: 668–76.

Tsai J, Grutzendler J, Duff K, Gan WB. Fibrillar amyloid deposition leads to local synaptic abnormalities and breakage of neuronal branches. Nat Neurosci 2004; 7: 1181–3.

Ujiie M, Dickstein DL, Carlow DA, Jefferies WA. Blood-brain barrier permeability precedes senile plaque formation in an Alzheimer disease model. Microcirculation 2003; 10: 463–70.

Usui K, Hulleman JD, Paulsson JF, Siegel SJ, Powers ET, Kelly JW. Site-specific modification of Alzheimer's peptides by cholesterol oxidation products enhances aggregation energetics and neurotoxicity. Proc Natl Acad Sci USA 2009; 106: 18563–8.

Vana L, Kanaan NM, Hakala K, Weintraub ST, Binder LI. Peroxynitrite-induced nitrative and oxidative modifications alter tau filament formation. Biochemistry 2011; 50: 1203–12.

Westphalen RI, Scott HL, Dodd PR. Synaptic vesicle transport and synaptic membrane transporter sites in excitatory amino acid nerve terminals in Alzheimer disease. J Neural Transm 2003; 110: 1013–27.

Williams JA, Hyland R, Jones BC, Smith DA, Hurst S, Goosen TC, et al. Drug-drug interactions for UDP-glucuronosyltransferase substrates: a pharmacokinetic explanation for typically observed low exposure (AUCi/AUC) ratios. Drug Metab Dispos 2004; 32: 1201–8.

Yao PJ, Zhu M, Pyun EI, Brooks AI, Therianos S, Meyers VE, et al. Defects in expression of genes related to synaptic vesicle trafficking in frontal cortex of Alzheimer's disease. Neurobiol Dis 2003; 12: 97–109.

Zipser BD, Johanson CE, Gonzalez L, Berzin TM, Tavares R, Hulette CM, et al. Microvascular injury and blood-brain barrier leakage in Alzheimer's disease. Neurobiol Aging 2007; 28: 977–86.

Protection of primary neurons and mouse brain from Alzheimer's pathology by molecular tweezers

A. Attar[1,5], C. Ripoli[8], E. Riccardi[8], P. Maiti[1], D. D. Li Puma[8], T. Liu[1], J. Hayes[1], M. R. Jones[1,7], K. Lichti-Kaiser[10], F. Yang[1,7], G. D. Gale[3], C. Tseng[4], M. Tan[2], C. Xie[2,5], J. L. Straudinger[10], F. Klärner[9], T. Schrader[9], S. A. Frautschy[1,7], C. Grassi[8] and G. Bitan[1,5,6]

[1]Department of Neurology,
[2]Department of Psychiatry and Biobehavioral Sciences,
[3]Department of Molecular and Medical Pharmacology, and
[4]Department of Medicine, David Geffen School of Medicine,
[5]Brain Research Institute, and
[6]Molecular Biology Institute, University of California at Los Angeles, Los Angeles 90095, CA, USA;
[7]Greater Los Angeles Healthcare System, Veterans Hospital, North Hills 91343, CA, USA;
[8]Institute of Human Physiology, Università Cattolica, Rome 00168, Italy;
[9]Institute of Organic Chemistry, University of Duisburg-Essen, Essen 45117, Germany;
[10]Department of Pharmacology and Toxicology, University of Kansas, Lawrence 66045, KS, USA.

Supplementary Methods:

Animals: Surgical and all other procedures performed at University of California-Los Angeles were compliant with the National Research Council Guide for the Care and Use of Laboratory Animals, approved by the University of California-Los Angeles Institutional Animal Care Use Committee, and performed with strict adherence to the guidelines set out in the National Institutes of Health *Guide for the Care and Use of Laboratory Animals* at the Greater Los Angeles Veterans Affairs Healthcare System. Experiments performed in the Catholic University of Rome complied with Italian Ministry of Health guidelines, with national laws (Legislative decree 116/1992) and with European Union guidelines on animal research (No. 86/609/EEC). At University of California-Los Angeles, pregnant E18 Sprague–Dawley rats for primary neuronal culture experiments were purchased from Charles River Laboratory (Wilmington, MA) and triple-transgenic mice were bred in-house. In the Catholic University of Rome, Wistar rats and C57Bl/6 mice were bred in-house. Animals were kept on a standard diet and 12 h light/dark cycle with food and water provided *ad libitum*.

Selection of Aβ42 concentrations for synaptotoxicity experiments: For dendritic-spine experiments, we looked for relatively harsh conditions, which would induce robust spine retraction. Preliminary experiments using 10 μM Aβ42 led to substantial cell death that did not allow reliable quantitation of dendritic spine density, whereas 3 μM Aβ42 produced spine retraction and abundant varicosities without overt cell death, as shown in Figure 1, enabling evaluation of the protective effect of CLR01.

Similarly, for electrophysiologic experiments, we tested Aβ concentrations in the nanomolar range based on data from our and other groups demonstrating that 200 nM Aβ42 produced inhibition of synaptic transmission and plasticity of sufficient magnitude for measuring a potential rescuing action of CLR01 (see Supplementary Discussion below for a number of references supporting the selection of this concentration). In our experience, concentrations slightly lower than 200 nM produce impairment of the synaptic function that is too small and does not allow detecting statistically significant changes following CLR01 treatments. Moreover, several papers by Arancio and co-workers have shown that picomolar Aβ concentrations actually enhance long-term potentiation (LTP) rather than inhibiting it (Puzzo and Arancio, 2012, Puzzo *et al.* , 2011, Puzzo *et al.* , 2008).

Autaptic neuron culture preparation: Rat cortical astrocytes were plated onto glass coverslips (coated with agarose and sprayed with a mixture of poly-D-Lys and collagen 3 days before plating) in Dulbecco's Modified Eagle Medium supplemented with 10% fetal bovine serum and antibiotics. After 4–6 days, half the medium volume was replaced with neurobasal medium consisting of 2% B27, 0.5% L-Gln, and 1% penicillin-streptomycin-neomycin antibiotic mixture. One day later, hippocampal neurons from P0–P2 Wistar rat brains were suspended in neuronal medium and plated at 25,000 per cm^2 onto the glial microislands. Two weeks later, autapses had formed and were ready to be studied. Every 4 days, half the neuronal medium volume was replaced with fresh neuronal medium supplemented with 2 μM cytosine arabinoside.

Patch-clamp recording: Currents were recorded using an Axopatch 200B amplifier (Molecular Devices), and the pCLAMP system (version 10, Molecular Devices) was used for data acquisition and analysis. Patch pipettes resistances were 3–4 MΩ when filled with intracellular solution consisting of (in mM): 136 KCl, 17.8 4-(2-hydroxyethyl)-1-

piperazineethanesulfonic acid, 1 ethyleneglycol tetraacetic acid, 0.6 $MgCl_2$, 4 ATP, 0.3 GTP, 12 creatine phosphate, and 50 U/ml phosphocreatine kinase. The extracellular solution contained (in mM): 140 NaCl; 2 KCl; 10 4-(2-hydroxyethyl)-1-piperazineethanesulfonic acid; 10 glucose; 4 $MgCl_2$; and 4 $CaCl_2$, pH 7.4. All experiments were performed at room temperature (23–25°C).

Hippocampal slice preparations: Coronal hippocampal slices (400-μm thick) were obtained from 8-weeks old male C57BL/6 mice according to standard procedures (Ripoli *et al.*, 2012). Brain slices were cut using a vibratome (VT1000S, Leica Microsystems) and incubated in the cutting solution containing (in mM): 124 NaCl, 3.2 KCl, 1 NaH_2PO_4, 26 $NaHCO_3$, 2 $MgCl_2$, 1 $CaCl_2$, 10 glucose, 2 Na-pyruvate, and 0.6 ascorbic acid (pH 7.4, 95% O_2/5% CO_2) for at least 60 min at 30–32°C, and then stored in the same solution at room temperature until use.

Long-term potentiation recordings: During the electrophysiological recordings, slices were perfused with artificial cerebrospinal fluid (artificial CSF; in mM): 124 NaCl, 3.2 KCl, 1 NaH_2PO_4, 1 $MgCl_2$, 2 $CaCl_2$, 26 $NaHCO_3$, and 10 glucose (pH 7.4, 95% O_2/5% CO_2) maintained at 30–32°C by an in-line solution heater and temperature controller (TC-344B, Warner Instruments) in a submerged recording chamber. Data acquisition and stimulation protocols were performed with the Digidata 1440 Series interface and pClamp 10 software (Molecular Devices). To study synaptic transmission, we measured the peak amplitudes of field excitatory postsynaptic potentials (fEPSPs) elicited by stimuli of increasing amplitudes, before and after slice exposure to artificial CSF containing either 200 nM freshly prepared Aβ42 or the same amount of dimethyl sulfoxide contained in the Aβ42 solutions (vehicle) in the absence or presence of 10-fold excess MTs, and plotted input/output (I/O) curves. The stimulation intensity that produced one-third of the maximal response was used for the test pulse and tetanus. After 20–30 min of stable baseline responses to test stimulations delivered once every 20 s, LTP was induced with a standard high-frequency stimulation paradigm consisting of four trains of 50 stimuli at 100 Hz (500 ms each) repeated every 20 s. Responses to test pulses then were recorded every 20 s for 60 min to measure LTP. The magnitude of LTP was measured 60 min after tetanus and expressed as a percentage of baseline fEPSP peak

amplitude. Reported fEPSP amplitudes at 60 min are averages from recordings obtained during the last 5 min of post-tetanus recordings.

Analysis of Aβ42 peptide by SDS and native PAGE/western blotting: The Aβ42 solutions for SDS-PAGE analysis were mixed with NuPAGE® LDS sample buffer 4× (at the final Aβ concentration of 200 nM) and separated on 10–20% gradient *Novex®* *Tricine* precast gels (Invitrogen) according to the manufacturer's protocol. Native PAGE was performed using 10–20% gradient Tris–glycine precast gels (Invitrogen). Native sample buffer 2× (Invitrogen) was added to the samples (at the final Aβ concentration of 200 nM) and samples then were electrophoresed in native buffer (Invitrogen) at 125 V. After electrophoresis under denaturing or non-denaturing conditions, the proteins were transferred to 0.2-μm nitrocellulose membranes (Amersham Biosciences, Buckinghamshire, UK). Membranes were blocked for 1 h, at room temperature, in a suspension of 5% non-fat milk in Tris-buffered saline containing 0.1% Tween-20 prior to incubation overnight at 4 °C with mAb 6E10 (Signet, Dedham, MA, USA; 1:1000). Membranes were washed 3 times with Tris-buffered saline containing 0.1% Tween-20 and then incubated with horseradish peroxidase-conjugated anti-mouse secondary antibody (Cell Signaling; 1:2000) at room temperature for 1 h. Development was done after 5 minutes of incubation with enhanced chemiluminescence reagents (SuperSignal west Femto Pierce) and exposed to Hyperfilm (Amersham Biosciences). Molecular sizes for immunoblot analysis were determined using a ColorBurst™ Electrophoresis Marker (Sigma-Aldrich) and Rainbow molecular weight markers (Amersham Biosciences). The bovine serum albumin was stained with Coomassie Blue (Sigma-Aldrich) to approximate the molecular weight in native conditions.

Immunohistochemistry controls: Immunohistochemistry for all treatment groups was performed simultaneously and analysis of slides was randomized. Adjacent slides treated similarly except in the absence of a primary antibody were evaluated as negative controls.

Linear mixed effects model for immunohistochemistry statistical analysis: Linear mixed effects models were used to evaluate the treatment effect on the outcome of Aβ, and p-tau load. Specifically, treatment groups, litters, and brain areas were included as the fixed effects and the random intercept was included as the random effect to

account for the correlation among multiple measurements from the same mice. In the models, different areas of the brain also were allowed to have different variance in the random effects. The estimated treatment effect was calculated for the total brain and each brain area.

Supplementary Results:

* 1 h pre-incubation of Aβ42 with CLR01
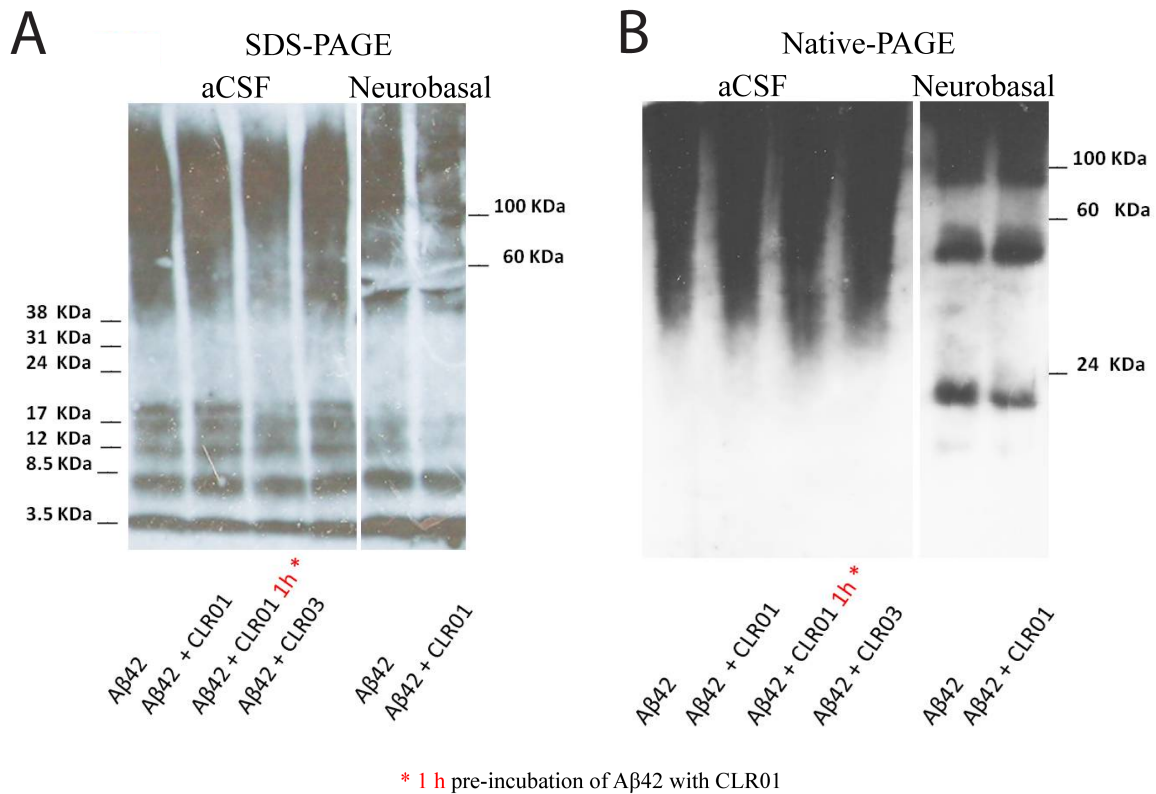
Supplementary Figure S1. Assembly size distribution pattern of Aβ42 preparations in the absence or presence of MTs. Preparations of Aβ42 alone, Aβ42 + CLR01, Aβ42 + CLR01 incubated for 1 h or Aβ42 + CLR03 in artificial CSF or neurobasal media were fractionated using SDS-PAGE (A) or native-PAGE (B) and then analyzed by Western blot using mAb 6E10.

CLR01 caused minor changes in the assembly size distributions, generally characterized by moderately decreasing the abundance of mid-size oligomers and increasing the abundance of larger assemblies.
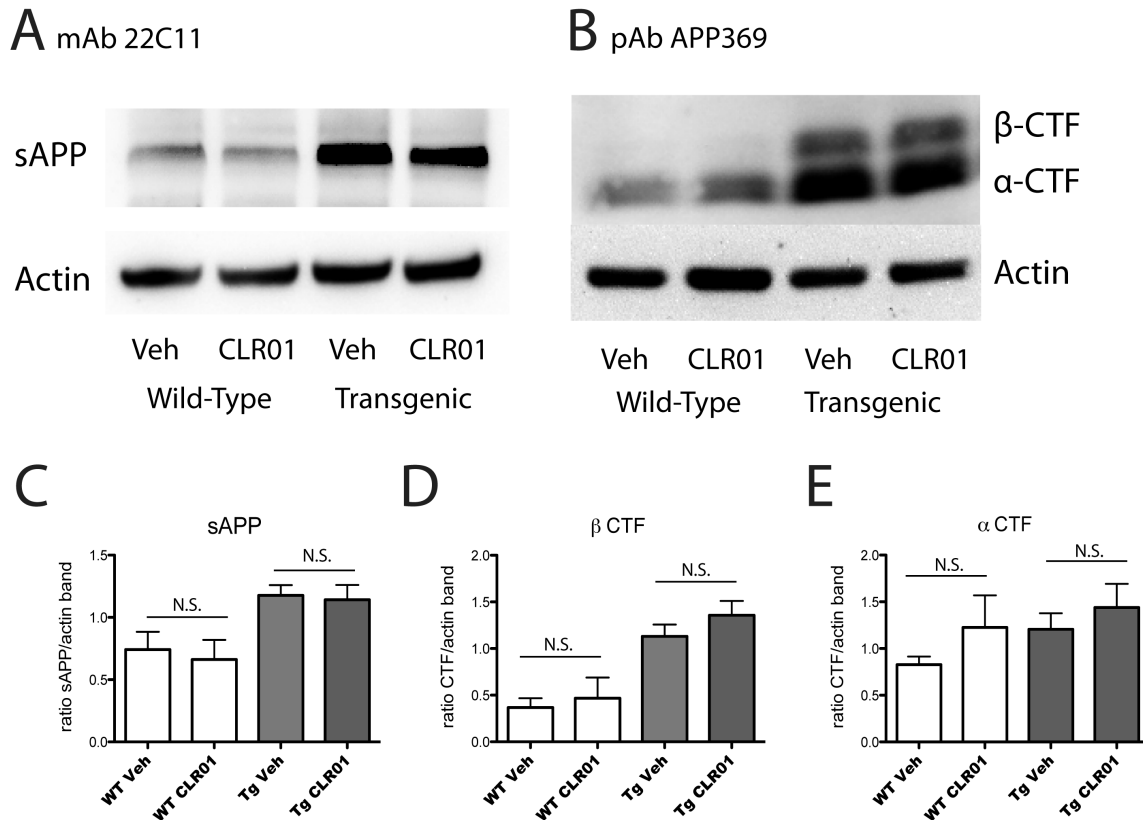
Supplementary Figure S2. No difference in levels of sAPP, CTF-α, or CTF-β with CLR01 treatment. Soluble and detergent-soluble fractions of brain extracts from vehicle- or CLR01-treated wild-type or transgenic mice were subjected to Western blot analysis. A) N-terminal APP antibody 22C11 used to assess levels of sAPP. B) C-terminal APP antibody APP369 used to assess levels of CTF-α and CTF-β. Densitometric analysis of Western blots for C) sAPP; D) CTF-β; and E) CTF-α was calculated after normalizing to the actin loading control. Wild-type (WT) Veh $n = 4$, wild-type CLR01 $n = 4$, transgenic (Tg) Veh $n = 12$, transgenic CLR01 $n = 10$.

Supplementary Discussion:

When comparing the level of potentiation or inhibition of potentiation in the literature, it is important to remember that LTP depends on several factors, including the paradigm used to elicit potentiation, the animals employed (mice or rats) and their age, the bath temperature and the synaptic pathway investigated (perforant, mossy fiber, or

Schaffer collateral pathways). Our findings that 200 nM Aβ42 markedly inhibited but did not abolish LTP are in agreement with the reports of similar experimental procedures (Berman *et al.* , 2008, Du *et al.* , 2008, Oliveira *et al.* , 2010). In our hands, 200 nM Aβ42 decreased LTP at the CA3–CA1 synapses to approximately half its normal value, reducing the fEPSP amplitude potentiation from $115.0 \pm 8.8\%$ to $53.7 \pm 5.1\%$.

Comparison between experiments conducted by different groups is not always straightforward because of the different experimental settings used. For example, stronger inhibition of LTP has been observed in previous work (Kessels *et al.* , 2010, Lambert *et al.* , 1998, Lauren *et al.* , 2009, Wang *et al.* , 2004), in which the concentrations of Aβ42 used were higher than those used in our experiments (500 nM vs. 200 nM, respectively). Wang et al. reported that "synthetic Aβ inhibited the induction of NMDAR-dependent LTP *in vitro*, with a threshold concentration of Aβ of 100–200 nM and a strong inhibition by 500 nM Aβ" (Wang *et al.* , 2004). Lambert et al. (Lambert *et al.* , 1998) used different animals (P21 rats), different Aβ oligomer concentrations (500 nM), different Aβ42 exposure time (45 min) and a different protocol for the LTP induction (a single tetanus consisting of 100 Hz, 2 s, 200 μs) from those reported in our paper. Moreover, in the work of Wang et al. (Wang *et al.* , 2004), LTP was performed in the dentate gyrus of rat brain slices whereas our paper investigated the CA3–CA1 synapses in mouse hippocampal slices. Interestingly, the Aβ42 preparations used by Kessels et al. (Kessels *et al.* , 2010) and Lauren et al. (Lauren *et al.* , 2009) reportedly had distinct effects on synaptic plasticity despite the two groups using the same Aβ concentration, the same strain of mice and the same paradigm to induce LTP.

Finally, Aβ-induced changes in synaptic function have been attributed to their effects on post-synaptic processes (Lacor *et al.*, 2004), presynaptic functions (Kelly *et al.*, 2005, Parodi *et al.*, 2010, Zhang *et al.*, 2009), or both (Ting *et al.*, 2007). The heterogeneous conclusions reached in different studies reflect the use of different experimental approaches, various animal models, a broad range of Aβ concentrations, different protocols for preparing Aβ oligomers, and different time windows for evaluating synaptic effects. Consequently, some groups have found that Aβ had no effect on basal synaptic transmission (Chapman *et al.*, 1999, Malinow *et al.*, 2008, Stern *et al.*, 2004, Wang *et al.*, 2004) whereas others have observed marked synaptic depression, with (Kessels *et al.*, 2010) or without LTP deficits (Hsia *et al.*, 1999). In light of these considerations, it is not surprising that a range of results has been observed by different groups measuring the inhibitory effects of Aβ42 treatment in brain slices.

References:

Berman DE, Dall'Armi C, Voronov SV, McIntire LB, Zhang H, Moore AZ, et al. Oligomeric amyloid-β peptide disrupts phosphatidylinositol-4,5-bisphosphate metabolism. Nat Neurosci. 2008 May;11(5):547-54.

Chapman PF, White GL, Jones MW, Cooper-Blacketer D, Marshall VJ, Irizarry M, et al. Impaired synaptic plasticity and learning in aged amyloid precursor protein transgenic mice. Nat Neurosci. 1999 Mar;2(3):271-6.

Du H, Guo L, Fang F, Chen D, Sosunov AA, McKhann GM, et al. Cyclophilin D deficiency attenuates mitochondrial and neuronal perturbation and ameliorates learning and memory in Alzheimer's disease. Nat Med. 2008 Oct;14(10):1097-105.

Hsia AY, Masliah E, McConlogue L, Yu GQ, Tatsuno G, Hu K, et al. Plaque-independent disruption of neural circuits in Alzheimer's disease mouse models. Proc Natl Acad Sci USA. 1999;96(6):3228-33.

Kelly BL, Vassar R, Ferreira A. β-amyloid-induced dynamin 1 depletion in hippocampal neurons. A potential mechanism for early cognitive decline in Alzheimer disease. J Biol Chem. 2005 Sep 9;280(36):31746-53.

Kessels HW, Nguyen LN, Nabavi S, Malinow R. The prion protein as a receptor for amyloid-β. Nature. 2010 Aug 12;466(7308):E3-4; discussion E-5.

Lacor PN, Buniel MC, Chang L, Fernandez SJ, Gong Y, Viola KL, et al. Synaptic targeting by Alzheimer's-related amyloid β oligomers. J Neurosci. 2004 Nov 10;24(45):10191-200.

Lambert MP, Barlow AK, Chromy BA, Edwards C, Freed R, Liosatos M, et al. Diffusible, nonfibrillar ligands derived from $A\beta_{1-42}$ are potent central nervous system neurotoxins. Proc Natl Acad Sci USA. 1998;95(11):6448-53.

Lauren J, Gimbel DA, Nygaard HB, Gilbert JW, Strittmatter SM. Cellular prion protein mediates impairment of synaptic plasticity by amyloid-β oligomers. Nature. 2009 Feb 26;457(7233):1128-32.

Malinow R, Hsieh H, Wei. W. Impact of β amyloid on excitatory synaptic transmission and plasticity. Synaptic Plasticity and the Mechanism of Alzheimer's Disease. Berlin Heidelberg: Springer-Verlag; 2008. p. 63-8.

Oliveira TG, Chan RB, Tian H, Laredo M, Shui G, Staniszewski A, et al. Phospholipase d2 ablation ameliorates Alzheimer's disease-linked synaptic dysfunction and cognitive deficits. J Neurosci. 2010 Dec 8;30(49):16419-28.

Parodi J, Sepulveda FJ, Roa J, Opazo C, Inestrosa NC, Aguayo LG. β-amyloid causes depletion of synaptic vesicles leading to neurotransmission failure. J Biol Chem. 2010 Jan 22;285(4):2506-14.

Puzzo D, Arancio O. Amyloid-β Peptide: Dr. Jekyll or Mr. Hyde? J Alzheimers Dis. 2012 Jun 26.

Puzzo D, Privitera L, Fa M, Staniszewski A, Hashimoto G, Aziz F, et al. Endogenous amyloid-β is necessary for hippocampal synaptic plasticity and memory. Ann Neurol. 2011 May;69(5):819-30.

Puzzo D, Privitera L, Leznik E, Fa M, Staniszewski A, Palmeri A, et al. Picomolar amyloid-β positively modulates synaptic plasticity and memory in hippocampus. J Neurosci. 2008 Dec 31;28(53):14537-45.

Ripoli C, Piacentini R, Riccardi E, Leone L, Li Puma DD, Bitan G, et al. Effects of different amyloid β-protein analogues on synaptic function. Neurobiol Aging. 2012:In press.

Stern EA, Bacskai BJ, Hickey GA, Attenello FJ, Lombardo JA, Hyman BT. Cortical synaptic integration in vivo is disrupted by amyloid-β plaques. J Neurosci. 2004 May 12;24(19):4535-40.

Ting JT, Kelley BG, Lambert TJ, Cook DG, Sullivan JM. Amyloid precursor protein overexpression depresses excitatory transmission through both presynaptic and postsynaptic mechanisms. Proc Natl Acad Sci USA. 2007 Jan 2;104(1):353-8.

Wang Q, Walsh DM, Rowan MJ, Selkoe DJ, Anwyl R. Block of long-term potentiation by naturally secreted and synthetic amyloid β-peptide in hippocampal slices is mediated via activation of the kinases c-Jun N-terminal kinase, cyclin-dependent kinase 5, and p38 mitogen-activated protein kinase as well as metabotropic glutamate receptor type 5. J Neurosci. 2004 Mar 31;24(13):3370-8.

Zhang W, Miao J, Hao J, Li Z, Xu J, Liu R, et al. Protective effect of S14G-humanin against β-amyloid induced LTP inhibition in mouse hippocampal slices. Peptides. 2009 Jun;30(6):1197-202.